Integrating propagation and recovery dynamics into groundwater drought vulnerability assessment through exposure, pressure, and aquifer system response.

Katarzyna Sawicka[1], Klaudia Jurzyk[1]

[1]Faculty of Geology, University of Warsaw, Żwirki i Wigury Street, 93, 02-089 Warsaw, Poland

Correspondence to: Katarzyna Sawicka (sawicka@uw.edu.pl)

Abstract. ~~Groundwater drought is influenced more by system-specific response dynamics than by meteorological forcing alone. We introduce a multi-scale framework that combines exposure, pressure, and sensitivity with process-based metrics of drought propagation and recovery to assess groundwater drought vulnerability. The Drought Impact Potential Index (DIPI) is developed and tested across a regional aquifer system. Propagation probability, median recovery time, and resilience metrics are examined across temporal scales and in groundwater systems at different depths. The findings reveal that spatial vulnerability patterns are driven by variations in system memory and response time. Deeper aquifer systems tend to have higher propagation probability, longer recovery periods, and increased vulnerability, indicating delayed responses and persistent drought signals. Conversely, shallower systems respond more quickly and recover faster, leading to lower drought persistence. The spatial distribution of DIPI remains consistent whether using weighted or unweighted versions, confirming that the identified patterns are robust and reflect fundamental hydrogeological controls. These results demonstrate that groundwater drought vulnerability arises from interactions between external forcing and internal system dynamics and cannot be understood solely through static indicators. An area-based analysis of exposure–pressure contrast shows that 60.4% of the study area is dominated by the intrinsic system response, compared to 21.8% driven primarily by human pressure. The proposed framework offers a process-based approach for groundwater drought assessment and can be applied to other diverse aquifer systems.~~ Groundwater drought reflects the combined influence of meteorological forcing, aquifer memory, hydraulic connectivity, and anthropogenic modification. This study develops a hydrogeologically informed statistical framework that integrates temporal groundwater-drought characteristics with spatial indicators of Exposure, Pressure, and environmental Sensitivity. Standardized Precipitation and Groundwater Level Indices were analysed at 3-, 6-, and 12-month aggregation scales for 16 piezometers grouped into shallow unconfined, intermediate confined, and deep confined aquifer systems. The shallow unconfined aquifer showed the strongest SPI–SGI association, whereas the deep confined aquifer exhibited weaker correlations, longer drought persistence, and no observed recovery within the available record. These contrasts are consistent with differences in aquifer memory and hydraulic conditions, but conclusions concerning the deep system remain exploratory because it is represented by only two monitoring wells and may also be affected by sustained anthropogenic pressure. The Drought Impact Potential Index (DIPI) combines piezometer-level SGI-12 drought-response metrics with proxy indicators of groundwater abstraction, mining influence, groundwater-dependent ecosystems, and groundwater quality. Weighted and equally weighted formulations produced broadly similar regional patterns, although leave-one-out cross-validation indicated substantial interpolation uncertainty. The resulting maps should therefore be interpreted as exploratory screening products rather than predictive vulnerability maps. The E−P contrast describes only the relative mapped magnitudes of Exposure and Pressure and does not provide causal attribution of climatic and anthropogenic controls.

1 Introduction

Groundwater drought is increasingly recognized as a critical component of hydrological extremes, with impacts extending beyond water supply to ecosystems and water-dependent sectors. Unlike meteorological drought, groundwater drought reflects the integrated response of subsurface storage and flow processes, typically exhibiting delayed onset, attenuation of short-term variability, and prolonged persistence (Van Loon, 2015; Bloomfield ~~&~~and Marchant, 2013). As a result, groundwater drought cannot be interpreted as a direct response to precipitation deficits, but must be understood in the context of aquifer properties, recharge processes, and system memory.

Previous studies have demonstrated that the propagation of meteorological drought into groundwater is highly variable and strongly controlled by hydrogeological conditions, including storage capacity, hydraulic connectivity, and recharge mechanisms (Barker et al., 2016; Bloomfield et al., 2019~~).~~; Chen et al., 2024). Groundwater systems generally exhibit the longest and most complex response times within the hydrological cycle, reflecting the cumulative nature of subsurface processes and delayed transmission of climatic signals (Zhu et al., 2022; Teutschbein et al., 2025). In particular, deeper and more confined aquifers tend to filter short-term variability and respond primarily to prolonged forcing, whereas shallow systems remain more directly coupled to atmospheric conditions.

A key feature of groundwater drought is the asymmetry between propagation and recovery processes. While propagation depends on the accumulation of meteorological deficits, recovery requires sustained recharge and is therefore typically slower and more constrained, particularly in systems with high storage capacity (Van Loon et al., 2016; Thomas ~~&~~and Famiglietti, 2017). This asymmetry leads to persistent groundwater deficits even after meteorological conditions improve, explaining the decoupling between meteorological and groundwater drought signals observed in many regions.

In human-modified environments, groundwater drought dynamics are further influenced by anthropogenic pressures such as groundwater abstraction and mining-related dewatering, which alter hydraulic gradients~~ and~~, storage conditions~~ (~~, and the broader sustainability of groundwater systems (Gorelick and Zheng, 2015; Van Loon et al., 2016). Recent studies indicate that groundwater drought may be driven either by climatic forcing or by human activities, depending on local conditions, with anthropogenic impacts often amplifying drought severity, duration, and recovery time (Gleeson et al., 2020; Jiao D. et al., 2020; Ghasempour et al., 2025). However, these effects are spatially heterogeneous and interact with intrinsic aquifer properties, making it difficult to disentangle the relative contribution of external forcing and internal system response.

Despite substantial progress in groundwater drought research, ~~existing approaches typically focus either on~~ temporal ~~dynamics (e.g., propagation and recovery~~drought-response analysis~~) or on~~ and spatial vulnerability assessment ~~using~~are commonly treated separately. Temporal studies focus on lag, attenuation, persistence, and recovery, whereas composite ~~indices. These perspectives are rarely integrated into a unified framework that explicitly links process-based system behavior with~~ spatial ~~patterns of drought impact. Moreover, widely used groundwater vulnerability frameworks are typically based on static indicators and expert-based weighting schemes, which, despite their practical applicability, do not explicitly represent process-based dynamics such as delayed recovery, threshold-type propagation, and system memory effects~~ indices generally combine hydrogeological, climatic, land-use, and anthropogenic indicators to assess groundwater drought vulnerability (Ling et al., 2023; Saha et al., 2021). ~~In contrast, process-based approaches explicitly account for the temporal dynamics of groundwater systems, linking drought propagation and recovery to aquifer properties and system memory, thereby providing~~Integrating these perspectives may support a more ~~physically grounded basis for assessing~~comprehensive, although still indicator-based, assessment of groundwater drought ~~vulnerability~~.

This study ~~addresses this gap by developing~~develops a ~~process-oriented~~hydrogeologically informed statistical framework that ~~integrates groundwater~~ links observed SPI–SGI relationships and SGI-derived drought ~~dynamics -~~-response metrics with a spatial assessment of drought impact potential. ~~We introduce a composite Drought Impact Potential Index (DIPI) that combines exposure, pressure, and system sensitivity~~The framework is not a numerical groundwater-flow model and does not explicitly ~~incorporates process-based metrics derived from groundwater drought characteristics. In addition, we propose a spatial contrast approach based on the difference between exposure and pressure (E − P), which enables disentangling the~~ simulate recharge, storage, or hydraulic parameters. DIPI is therefore presented as an exploratory screening index that integrates relative ~~influence of intrinsic system response and anthropogenic forcing on the spatial distribution of groundwater drought impact~~Exposure, Pressure, and Sensitivity scores.

The objectives ~~of this study~~ are to: (1) quantify groundwater drought dynamics across multiple temporal scales ~~using standardized indices,~~; (2) ~~evaluate differences in propagation~~compare lag, persistence, and recovery ~~behavior between~~behaviour among the monitored aquifer systems ~~with contrasting hydrogeological characteristics,~~; and (3) ~~assess~~examine the relative spatial distribution of groundwater drought ~~impact potential by integrating exposure, pressure~~Exposure, anthropogenic Pressure, and ~~sensitivity components. By linking temporal drought dynamics with spatial vulnerability patterns, this study provides~~environmental Sensitivity. The E−P contrast is used only as a descriptive comparison of mapped component magnitudes and not as a ~~mechanistic basis for understanding groundwater drought in complex, human-impacted aquifer systems~~causal separation of natural and anthropogenic controls.

2 Study area

2.1 Location and general setting

The study was conducted within Groundwater Body No. 43 (PLGW600043; hereafter GWB 43), located in the Odra basin and extending across northern Greater Poland and parts of Kuyavia (Fig. 1). The unit covers approximately 3,666 km² and consists of a mosaic of agricultural landscapes, lake basins, and river valleys shaped by Late Pleistocene glaciations. The area features low relief, extensive sandy plains, and numerous depressions that promote groundwater–surface water interactions (~~GWB 43 status card~~PGI-NRI, 2022).

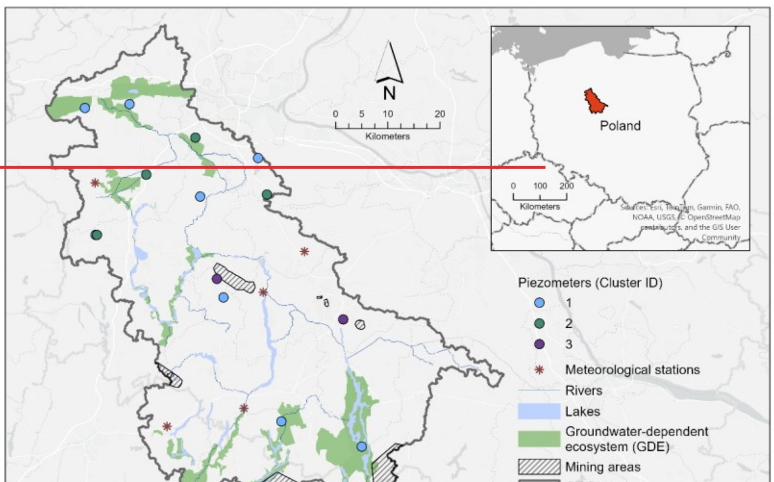

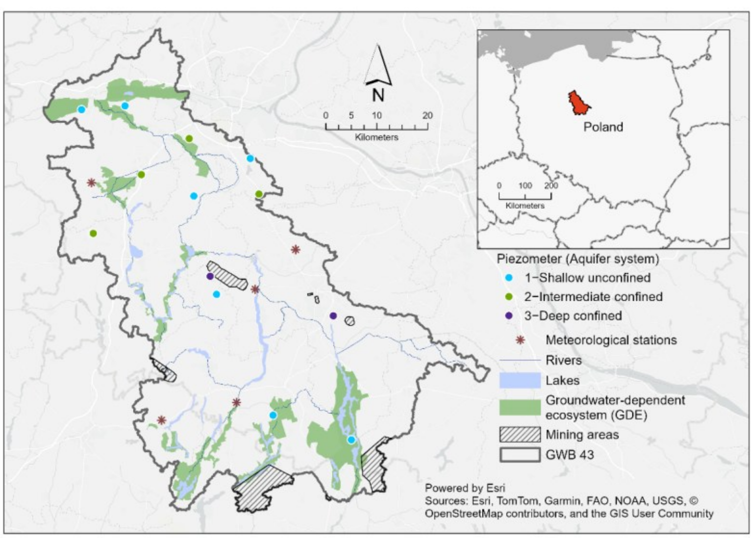

Figure 1: Study area and monitoring network within GWB 43. Location of GWB 43 (PLGW600043) in central-western Poland and spatial distribution of monitoring piezometers grouped into three aquifer systems. The figure includes hydrographic features, lakes, groundwater-dependent ecosystems (GDEs), and mining areas used in the spatial drought-impact framework.

2.2 Hydrogeological framework

GWB 43 comprises three principal aquifer systems: (1) shallow Quaternary sands and gravels, (2) Neogene–Paleogene sandy formations associated with lignite-bearing sequences, and (3) locally fractured Upper Cretaceous carbonates. Recharge of the shallow system occurs mainly through direct infiltration of precipitation, whereas the deeper aquifers are replenished by leakage through discontinuous clay layers and via hydraulic windows. Strong vertical connectivity between aquifers has been documented in several zones, particularly where mining drainage or river valleys modify the hydraulic gradient. This structural configuration results in a system that is sensitive to both climatic forcing and anthropogenic drainage (~~GWB 43 status card~~PGI-NRI, 2022).

Since 2012, national assessments have consistently classified GWB 43 as having poor quantitative and chemical status. Exceedances most often involve nitrate, ammonium, sulfate, and sodium, reflecting the combined impact of agricultural runoff, inadequate rural sanitation, and possible upconing of mineralized waters from deeper layers. Many monitoring wells lack protective low-permeability covers, further increasing their vulnerability to pollution and speeding up the transfer of surface signals into groundwater (The Polish Geological Institute - National Research Institute, 2022). These features are illustrated in the conceptual cross-section (Fig. 2).

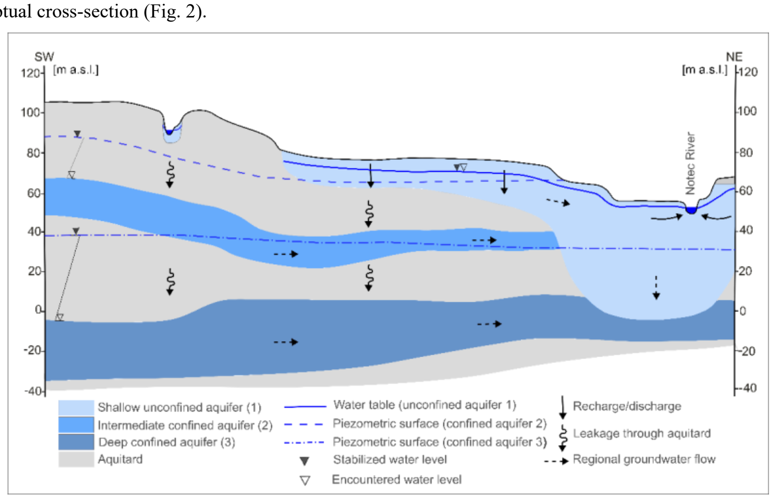

Figure 2: Conceptual hydrogeological cross-section of the GWB 43 aquifer system. Conceptual SW–NE cross-section illustrating the three principal aquifer systems in GWB 43: shallow unconfined, intermediate confined, and deep confined aquifers. The scheme highlights vertical hydraulic connectivity, leakage through aquitards, recharge/discharge zones, and dominant regional groundwater-flow directions that underpin differences in drought propagation and recovery

2.3 Anthropogenic pressures on groundwater systems

The groundwater system within GWB 43 faces significant human-induced stress from both groundwater extraction and mining activities. Based on available data, a total of 1267 groundwater-related features were identified in the study area, including 1247 abstraction wells and 20 dewatering wells linked to mining operations. The spatial distribution of groundwater abstractions and mining activities, along with the ~~normalized~~normalised pressure layers used in the DIPI framework, is shown in Appendix A (Fig. A1).

Groundwater abstraction is widespread and includes a range of uses, such as municipal water supply, agricultural abstraction, and individual wells serving local infrastructure (e.g., schools, healthcare facilities, and dispersed settlements). The spatial distribution of these wells is heterogeneous, with locally high densities reflecting areas of intensified water use.

In addition to abstraction, groundwater conditions are influenced by mining-related dewatering associated with open-pit operations. These activities generate local-to-regional-scale depression cones and modify hydraulic gradients, thereby affecting groundwater flow patterns and storage conditions (Fiszer, Derkowska-Sitarz, 2010; Przybyłek, 2018; Nowak et al., 2023).

The coexistence of widespread groundwater abstraction and localized high-intensity dewatering results in a complex pattern of anthropogenic pressure superimposed on natural hydrogeological conditions. This makes GWB 43 a representative example of a groundwater system where climatic forcing interacts with substantial human pressure, providing a suitable framework for analyzing the combined effects of system response and external stressors on groundwater drought dynamics.

The spatial distribution of these anthropogenic pressures is synthesized in the pressure component (P) and presented as a continuous surface in Fig. ~~6~~7, forming one of the key inputs to the DIPI framework.

3 Datasets

This study integrates groundwater-level, groundwater-chemistry, and precipitation datasets for the GWB 43 groundwater body. The objective was to characterize groundwater drought dynamics consistently across aquifer levels and to compare them with meteorological forcing.

3.1. Precipitation

Monthly precipitation totals were obtained from five meteorological stations operated by the Institute of Meteorology and Water Management – National Research Institute (IMGW-PIB): Gębice, Zalesie, Trzemeszno, Pakość and Jaksice. Continuous records covering 1986–2024 were used to compute the Standardized Precipitation Index (SPI) at monthly resolution, consistent with SGI calculations.

3.2. Groundwater

Groundwater-level records were obtained from the national monitoring network operated by the Polish Geological Institute – National Research Institute (Państwowy Instytut Geologiczny – Państwowy Instytut Badawczy; PIG-PIB) under the State Hydrogeological Service (Państwowa Służba Hydrogeologiczna; PSH), and by the Chief Inspectorate of Environmental Protection (Główny Inspektorat Ochrony Środowiska; GIOŚ) within the State Environmental Monitoring program (Państwowy Monitoring Środowiska; PMŚ). The hydrogeological and meteorological time series used in this study were partly derived from raw datasets compiled in an earlier MSc thesis focused on a preliminary groundwater drought assessment in GWB 43 (Jurzyk, 2025). In the present study, however, these input data were reprocessed within a substantially revised analytical framework, including a new expert-based piezometer classification, expanded event-based drought metrics, and the development of the Drought Impact ~~and Pressure~~Potential Index (DIPI). Sixteen monitoring wells within GWB 43 were selected and assigned to three hydrostratigraphic groups: unconfined, intermediate, and deep confined aquifers. Hydraulic heads were converted to monthly means and used to compute the Standardized Groundwater Level Index (SGI). Observation periods differed among piezometers, and several records contained missing months. The complete start and end dates, number of valid monthly observations, and data completeness for each piezometer are provided in Table 1. Missing groundwater-level observations were not interpolated. For each piezometer, trailing 3-, 6-, and 12-month aggregation windows were calculated only when all constituent calendar months were available. Consequently, the SGI series differ slightly in length among wells and aggregation scales. Key characteristics of the groundwater monitoring wells aggregated by aquifer type are summarised in Table 1. ~~Observation periods differ among wells; therefore, period limits refer to the earliest and latest observations available within each cluster.~~

Table 1: Characteristics of monitoring piezometers grouped by aquifer system in GWB 43.

Aquifer system	~~Piezometers~~Piezometer	~~Mean water-table depth~~ Screen interval (m b.g.l.)	~~Mean interval thickness (top – bottom,~~ Well depth (m b.g.l.)	Observation period	Valid monthly observations	Missing months	Com

Wstawione komórki

Wstawione komórki

Wstawione komórki

1 — ~~shallow~~ Shallow unconfined	II/1271/1~~II/906/1, II/908/1, II/908/2, II/1271/1, II/1272/1, II/1273/1, II/1274/1, II/1274/2, II/1276/1, II/1285/1~~	~~5.9~~4.05–12.10	~~5.9–17.3~~28.0	~~2005–2021~~2004-07–2024-04	228	10	95.8
	II/1272/1	3.00–4.60	5.5	2004-07–2020-10	196	0	100.0
	II/1273/1	1.86–19.00	19.0	2004-07–2024-04	235	3	98.7
	II/1274/1	4.36–23.00	23.0	2005-07–2024-04	225	1	99.6
	II/1274/2	4.36–23.00	23.0	2009-04–2021-05	146	0	100.0
	II/1276/1	5.30–13.50	19.0	2005-07–2024-04	226	0	100.0
	II/1285/1	14.00–29.00	29.0	2014-03–2024-04	122	0	100.0
	II/906/1	6.50–16.00	16.0	2006-06–2024-04	215	0	100.0
	II/908/1	7.60–16.50	16.5	2006-06–2020-05	168	0	100.0
	II/908/2	7.84–16.00	16.0	2006-06–2024-04	215	0	100.0
2 — ~~intermediate~~ Intermediate confined	~~II/521/1, II/527/1,~~ II/1272/2~~, II/1275/1~~	~~16.3~~20.00–22.00	~~16.3–28.3~~24.0	~~1986~~2006-11–2024-04	210	0	
	II/1275/1	3.00–6.50	19.0	2005-07–2024-04	226	0	100.0
	II/521/1	28.00–41.50	41.5	1985-11–2024-03	448	13	97.2
	II/527/1	14.00–43.00	43.0	1985-07–2024-03	462	3	99.4
3 ~~— deep~~ Deep confined	~~II/797/1,~~ II/1065/1	~~68.0~~70.00–80.00	~~68.0–83~~82.0	~~1991~~1994-04–2024-03	355	5	
	II/797/1	66.00–86.00	90.0	1990-07–2024-04	405	1	[illegible]

Wstawione komórki
Wstawione komórki
Wstawione komórki
Wstawione komórki
Wstawione komórki
Wstawione komórki

Notes: Screen interval denotes the top and bottom of the monitored interval below ground level. Observation period is reported separately for each piezometer and spans the first to the last valid monthly observation. Completeness was calculated as the ratio of valid monthly observations to the expected number of months within the reported period. Missing groundwater-level observations were not interpolated.

The assignment of piezometers to three hydrogeological groups was defined a priori, based on stratigraphic position, confinement conditions, and typical groundwater-table depth. These groups represent three conceptually distinct groundwater systems ~~(~~: shallow unconfined, ~~confined,~~ intermediate confined, and deep confined~~).~~ aquifers. The ~~stability~~consistency of SGI responses across ~~3-, 6-, and 12-month aggregations indicates~~the three aggregation scales supports the interpretation that the observed differences ~~are linked to~~reflect contrasts in storage ~~capacity~~ and recharge connectivity~~,~~ rather than ~~to artefacts~~solely effects of temporal averaging.

Since the grouping is expert-based rather than statistical analysis, and the number of observation wells in confined horizons is limited (4 and 2 wells, respectively), the results should be viewed as characteristic of typical settings rather than as population-wide statistics for the entire aquifer. This limitation is somewhat offset by the internal consistency of SGI metrics across different indices and by agreement with the conceptual hydrogeological model. Future work should evaluate the stability of these groups with additional monitoring points and, where possible, use complementary statistical grouping methods.

Aquifer-group mean SGI series were calculated as the arithmetic mean of the available well-level SGI values for each month. To reduce changes in temporal network support, a monthly aquifer-group mean was calculated only when data were available from at least 50% of the wells assigned to that group and from at least two wells. This required a minimum of five wells for the shallow unconfined aquifer, two wells for the intermediate confined aquifer, and both wells for the deep confined aquifer. The number of wells contributing to each monthly mean was also recorded.

4. Methods

The conceptual model highlights differences in damping, lag, and memory effects, which are quantified using the drought metrics described below (Fig. 3).

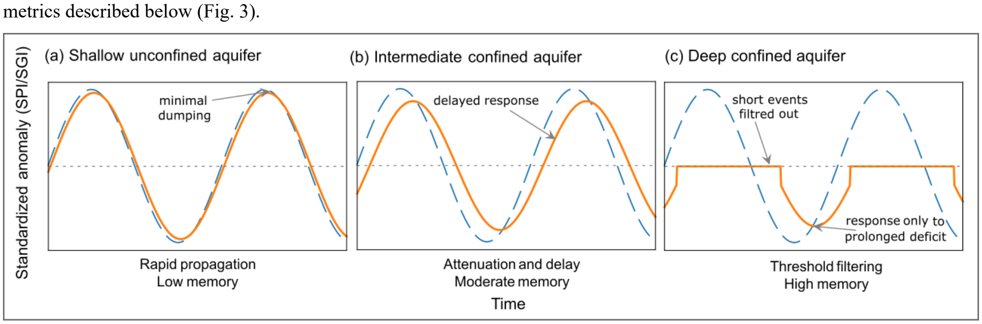

Figure 3: Conceptual model of groundwater drought propagation and recovery across aquifer systems. Schematic representation of SPI–SGI response ~~behavior~~behaviour across groundwater systems of increasing depth and memory. Dashed lines indicate meteorological forcing (SPI), whereas solid lines represent groundwater response (SGI): (a) rapid propagation in the shallow unconfined aquifer, (b) attenuated and delayed response in the intermediate confined aquifer, and (c) threshold-like response in the deep confined aquifer.

4.1 Standardized Precipitation Index (SPI)

The Standardized Precipitation Index (SPI) was used to quantify meteorological drought at multiple time scales. SPI expresses the deviation of precipitation from the long-term climatology in units of standard deviation, allowing comparison between stations and regions with different climates (McKee et al., 1993; Guttman, 1999; WMO, 2012).

SPI was used as a consistent indicator of precipitation deficit rather than as a complete representation of climatic water balance or effective groundwater recharge. It does not explicitly account for potential or actual evapotranspiration, temperature, soil-moisture dynamics, snow processes, or the timing and magnitude of recharge.

Monthly precipitation totals from the five IMGW-PIB stations were first aggregated to 3-, 6-, and 12-month moving sums to represent short-term, seasonal, and annual-scale water balance conditions, respectively. The cumulative distribution function G(Pk) was then transformed to the standard normal distribution:

$$SPI = \Phi^{-1}\big(G(P_k)\big), \tag{1}$$

where Φ^{-1} is the inverse standard normal cumulative distribution function.

Drought conditions were defined using commonly applied SPI thresholds (McKee et al., 1993; WMO, 2012). In this study, we adopt:

SPI < −1.0 moderate drought,

SPI < −1.5 severe drought,

SPI < −2.0 extreme drought.

For each time scale, drought events were identified as continuous periods during which SPI remained below a given threshold. For every event, we computed the duration (number of months), the minimum SPI value, and the accumulated severity (sum of SPI values below the threshold). These metrics were later compared with groundwater drought characteristics derived from SGI.

4.2 Standardized Groundwater Level Index (SGI)

~~The standardized groundwater index (SGI) was used to characterize groundwater drought conditions.~~ SGI was calculated ~~by standardizing~~separately for each piezometer and aggregation scale. Monthly groundwater levels were first aggregated using trailing 3-, 6-, and 12-month arithmetic means. An aggregation window was retained only when all constituent monthly observations were available; missing groundwater-level values were not interpolated.

To remove seasonality, the aggregated groundwater ~~level time series~~ level values were transformed separately for each calendar month using a non-parametric normal ~~-~~score transformation~~, as described by Bloomfield and Marchant (2013).~~:

$$\cancel{SGI_t = \Phi^{-1}(F(h_t)),} \quad SGI_{m,i} = \phi^{-1}\left(\frac{r_{m,i}-0.5}{n_m}\right), \tag{2}$$

where~~: F(h$_t$)~~ $r_{m,i}$ is the ~~cumulative distribution function~~rank of ~~monthly groundwater levels~~observation *i* among all available aggregated values for calendar month m, n_m is the number of valid observations for that month, and Φ^{-1} is the inverse standard normal cumulative distribution function. Average ranks were used for tied observations.

Drought conditions were defined as SGI < −1, with severity classes analogous to those used for SPI (Hisdal et al., 2001; Tallaksen ~~& Van Lanen, 2004).~~and Van Lanen, 2004). A drought event consisted of consecutive valid months below this threshold. A gap in the SGI series terminated an ongoing event. SGI describes standardized groundwater-level anomalies but does not independently identify their cause. In the human-modified GWB 43 system, negative SGI values may reflect the combined influence of meteorological drought, aquifer memory, groundwater abstraction, mining-related dewatering, and induced vertical leakage.

Both SPI and SGI were ~~analyzed~~analysed at consistent temporal scales to enable direct comparison of meteorological and groundwater drought dynamics (aggregation periods of 3, 6, and 12 months). Continuous periods below a given threshold were identified as drought events and summarised using standard drought metrics (see Section 4.3).

For aquifer-~~level~~system analyses, ~~individual~~aquifer-group mean SGI ~~time~~ series were ~~grouped by aquifer level (unconfined, intermediate, or deep). Aquifer level means of SGI were computed by averaging SGI values across all wells belonging to the same level for corresponding months. Aquifer-level SGI series~~calculated as described in Section 3.2 and were used to derive drought metrics ~~representative of each~~for comparison among the monitored aquifer ~~level.~~ systems.

Part of the raw groundwater-level and meteorological time series used in this study had previously been compiled within an earlier MSc-level assessment of groundwater drought in GWB 43 (Jurzyk, 2025). However, in the present study, all input data were reprocessed within a substantially revised analytical framework, including a new expert-based piezometer classification, expanded event-based drought metrics, and the development of the Drought Impact ~~and Pressure~~Potential Index (DIPI). The methodological steps applied to derive these drought-response metrics and the final index are described in the following section.

4.3 Drought metrics

Based on the reprocessed monthly SGI-12 time series and the updated piezometer grouping, a set of event-based drought metrics was calculated to quantify groundwater system response, including vulnerability, maximum drought duration, resistance, resilience, propagation probability, and median recovery time. Drought events were defined as continuous periods with SGI < −1.0, and a set of metrics describing duration, severity, propagation and recovery was derived following established approaches (Van Loon, 2015; Peters et al., 2003; Thomas ~~& Famiglietti, 2017).~~and Famiglietti, 2017). Drought metrics were calculated for both individual piezometer SGI series and aquifer-group mean SGI series. The well-level metrics were used as inputs to the spatial Exposure analysis, whereas the group-level metrics were used to compare temporal drought behaviour among aquifer systems.

The full set of applied drought metrics, together with their definitions and calculation formulas, is summarised in Table 2.

Table 2: Definitions and formulas of event-based groundwater drought metrics derived from SGI.

Metric	Symbol	Definition	Formula
Number of drought events	N	Total number of independent drought events (SGI < ~~=~~-1).	$N = J$
Duration	~~D~~D_j	Length of ~~a~~ drought event j in months.	$D_j = t_{end,j} - t_{start,j} + 1$
Severity	~~S~~S_j	~~Cumulative~~Signed cumulative SGI ~~deficit~~anomaly during ~~an~~drought event j.	$S_j = \sum_{t \epsilon J_j} SGI_t$
Mean severity	S_{mean}	Average signed cumulative severity across all drought events.	$S_{mean} = \frac{1}{J}\sum_{j=1}^{J} S_j$
Mean intensity	~~I~~I_j	Mean SGI value during drought ~~events~~event j.	$I_j = \frac{1}{D_j}\sum_{t \epsilon J_j} SGI_t$
Minimum SGI	SGI_{min}	~~The most~~Most negative SGI value in the time series.	$SGI_{min} = \cancel{\min (SGI_t} min_t\ (SGI_t)$
Resistance	CRT	~~Ability to avoid entering~~Fraction of valid months outside groundwater drought conditions.	$CRT = 1 - \cancel{\frac{\sum_{t=1}^{T} D_t}{\sum_{=t=0}^{T} Z_t}} \frac{\sum_{t=1}^{T} D_t}{T}$
Resilience	CRS	~~Probability~~One-step probability of ~~recovery~~transition from drought~~.~~ to non-drought conditions. CRS =	$CRS = \cancel{\frac{\sum_t W_t}{T - \sum_t Z_t}} \frac{\sum_{t=1}^{T-1} W_t}{\sum_{t=1}^{T-1} D_t}$
Vulnerability	VUL	Maximum absolute cumulative SGI deficit across drought events.	$\mathrm{VUL} = \max_j \sum_{t \epsilon J_j} \lvert \mathrm{SGI}_t \rvert$
Propagation probability	P	~~Probability that short-term groundwater drought propagates into long-term groundwater drought.~~Fraction of SGI-3 drought events matched to an overlapping SGI-12 drought event or to a subsequent SGI-12 event beginning within 12 months of the SGI-3 event onset. Each SGI-3 event is counted only once.	$P = \frac{N_{SGI3 \to SGI12}}{N_{SGI3}}$
~~Propagation lag~~	~~L~~	~~Most frequent delay between SPI and SGI drought onset.~~	$\cancel{L = mode(t_{start,j}^{SGI} - t_{start,j}^{SPI})}$
Recovery time	~~R~~R_j	Time ~~required~~from the minimum of event j to ~~return to near-normal conditions (~~the first subsequent month with SGI ≥ ~~=~~-0.5~~)~~.	$R_j = t_{rec,j} - t_{min,j}$

~~SGI, ~~Notes: SGI_t = Standardized Groundwater Level Index ~~(SGI)~~ at time t; t ~~–~~= time step (month); J ~~–~~= total number of drought events; J_j ~~–~~ = set of time steps belonging to drought event j; $t_{start,j}$ and $t_{end,j}$ ~~–~~= start and end of event j; $t_{min,j}$ ~~–~~= time of minimum SGI within event j; ~~$t^{SPI}_{start,j}$ – start time of the corresponding meteorological drought event;~~ $t_{rec,j}$ ~~– the~~ = first time step after the event minimum when SGI ~~≥~~ ≥ −0.5; ~~D,~~D_t = 1 if ~~SGI <~~SGI_t ≤ −1 and 0~~,~~ otherwise ~~0; Z~~; W_t = 1 if ~~SGI ≥~~D_t = 1 and D_{t+1} = 0, and 0~~,~~ otherwise ~~0; W = 1 if transition from drought to non-drought occurs~~; T ~~–~~= total number of valid time steps; N_{SGI3} ~~–~~ = number of short-term ~~(~~SGI-3~~)~~ groundwater drought events; $N_{SGI3 \rightarrow SGI12}$ – number of SGI-3 drought events ~~that develop into~~matched to an overlapping SGI-12 event or to an SGI-12 event beginning within 12 months of the SGI-3 event onset; each SGI-3 event is counted only once. VUL is the maximum absolute cumulative SGI deficit across drought events. CRS uses the drought threshold SGI ≤−1, whereas recovery time uses the near-normal threshold SGI ≥ −0.5.

The selected metrics collectively describe both the temporal characteristics of drought events and the dynamic response of groundwater systems, forming the basis for the exposure component of the Drought Impact Potential Index (DIPI) framework. **~~All statistical~~**Statistical analyses, SGI-based drought metrics, and **~~figure generation~~**time-series figures were **~~performed~~**produced in Python within the Google Colab environment using custom scripts. Spatial interpolation, raster processing, and map production were performed in ArcGIS Pro.

4.4 Lagged SPI–SGI correlation analysis

To examine ~~how~~ the temporal association between meteorological ~~drought spreads into~~ and groundwater drought, we ~~studied~~analysed the ~~relationships~~relationship between the Standardized Precipitation Index (SPI) and ~~the~~aquifer-group mean Standardized Groundwater Level Index (SGI) ~~across multiple aggregation periods (~~series at 3~~,~~-, 6~~,~~-, and 12~~ months), explicitly~~ -month aggregation scales, while accounting for delayed groundwater response (Bloomfield ~~&~~and Marchant, 2013; Barker et al., 2016~~).~~; Kumar et al., 2016). For each ~~groundwater cluster~~monitored aquifer system, SPI ~~data~~ was ~~taken~~obtained from the ~~nearest~~ precipitation station~~, based on geographic proximity~~ nearest to the ~~cluster~~ centroid~~.~~ of the corresponding piezometer group. This approach ~~preserves~~was intended to retain local precipitation variability relevant ~~for~~ to groundwater recharge~~, while spatially averaged precipitation can conceal drought timing and severity (Shukla & Wood, 2008; Vicente-Serrano et al., 2010).~~ that might be obscured by spatial averaging.

For each station~~–well~~aquifer-group pair~~,~~, and aggregation scale k, the contemporaneous Pearson correlation ~~coefficients were~~ coefficient was calculated ~~between SPIk and SGI~~as:

$$\cancel{r =} r_k(0) = corr\cancel{(SPI_k(t), SGI(t))}\ [SPI_k(t), SGI_k(t),] \quad (3)$$

where k ~~=~~ = 3,~~,~~ 6, ~~and~~or 12 months.

~~For each aggregation scale, Pearson correlation coefficients were computed between SPIk(t) and SGI(t), and then extended to lagged~~Lagged correlations were then calculated by shifting SGI relative to SPI over lags L=0–12 months:

~~$r(L)$~~ $r_k(L) = corr$ ~~$(SPI_k(t), SGI\ (t+L))$ where k = 3, 6, and 12 months.~~
~~The optimal lag for~~ $[SPI_k(t), SGI_k(t+L)],$ (4)

A positive value of L indicates that the groundwater signal follows the meteorological signal. Only temporally overlapping, non-missing SPI–SGI pairs were included in each ~~cluster and~~ correlation calculation.

For each aquifer system and aggregation scale ~~was identified as,~~ the lag associated with the highest ~~absolute correlation, indicating the main delay involved in recharge, storage~~positive Pearson correlation within the tested 0–12-month range was identified. Similar maximum-correlation approaches have been widely used to characterize the dominant temporal association between meteorological and groundwater drought indices, although the resulting optimal temporal association may vary among sites, aggregation scales, and ~~transit processes~~hydrogeological settings (Bloomfield ~~&~~and Marchant, 2013; ~~Barker et al., 2016; Chen et al., 2024).~~ Kumar et al., 2016). The identified lag was therefore interpreted as an empirical indicator of the strongest temporal association, rather than as a uniquely determined physical propagation time or a fixed aquifer response time. A maximum at L=12 months is consistent with the strongest correlation being found at the upper boundary of the tested range and does not rule out a longer response delay.

To assess whether the identified correlation maxima were stable over time, the lag analysis was repeated within moving 10-year windows, each shifted forward by 1 year. Within each window, Pearson correlations were calculated for lags of 0–12 months, and the lag associated with the maximum positive correlation was recorded. Only windows containing at least 96 valid paired monthly observations were retained. The moving-window analysis was used as a diagnostic sensitivity test of temporal stability, recognizing that the lag associated with the maximum correlation may vary among subperiods and may be influenced by serial dependence and changing climatic or anthropogenic conditions. It was not interpreted as an independent estimate of aquifer response time or as a formal confidence interval for the lag.

To evaluate ~~robustness against~~sensitivity to long-term co-trending, ~~analyses were~~the full-period analysis was also repeated ~~on~~using detrended ~~indices; interpretation depended on observing consistent~~ SPI and SGI series. Interpretation was based on the consistency of the general correlation and lag patterns ~~in both versions. A~~ between the original and detrended series. The complete ~~matrix of SPI–SGI correlations across different aggregation scales is available~~full-period correlation matrices are presented in Appendix B, whereas the moving-window stability analysis is shown in Appendix C, Figure C1.

4.5 Spatial analysis and Drought Impact Potential Index (DIPI)

This section represents the core methodological contribution of the study. To assess the spatial distribution of drought impact potential within GWB 43, we developed a composite Drought Impact Potential Index (DIPI) integrating exposure to groundwater drought, anthropogenic pressure, and system sensitivity. This approach is inspired by multidimensional and spatially explicit drought-vulnerability indices ~~in water resources and drought risk assessments (e.g., Tallaksen & Van Lanen, 2004; Van Loon~~ that integrate normalized environmental and anthropogenic indicators (Saha et al., ~~2016~~2021; Ling et al., 2023), and is adapted here to hydrogeological conditions.

~~Point attributes from monitoring piezometers (cluster ID, SGI-12 drought metrics) serve as primary spatial anchors. Continuous surface representations of drought performance (e.g., Vulnerability, Resilience) were generated through spatial interpolation (e.g., Inverse Distance Weighting, kriging) to enable comparison with other spatial drivers.~~ DIPI was developed as an exploratory spatial screening index intended to compare relative patterns within the study area. The selected component weights reflect expert judgment and were not calibrated against independent observations of groundwater-drought impacts.

For temporal comparison among aquifer systems, SGI series and drought metrics were summarized at the aquifer-group level. In contrast, the spatial Exposure analysis was based on drought metrics calculated independently for each of the 16 monitoring piezometers. Group-level metric values were not assigned to individual wells. For each piezometer, SGI-12 vulnerability (VUL), inverse resilience score (CRS_{inv}), and maximum drought duration (MaxDur) were calculated from its individual SGI-12 series. These well-level metrics were normalised across the monitoring network and interpolated separately within the GWB 43 boundary. The resulting continuous surfaces were subsequently combined according to the Exposure equation.

The piezometer-level SGI-12 metrics were interpolated separately using the Topo to Raster algorithm, with drainage enforcement disabled. Topo to Raster is based on an iterative finite-difference interpolation procedure related to a discretized thin-plate spline and was used here to generate continuous, smoothed surfaces from irregularly distributed monitoring points (Hutchinson, 1989). The same study-area boundary, raster extent, cell size, and snap raster were applied to all Exposure subcomponents to ensure spatial consistency among the resulting layers.

Interpolation performance was evaluated using leave-one-out cross-validation, a commonly used approach for assessing spatial interpolation accuracy when an independent validation dataset is unavailable (Li and Heap, 2008; Risk et al., 2022). Cross-validation was performed separately for normalized vulnerability (VUL'), inverse normalized resilience (CRS_{inv}'), and normalized maximum drought duration (MaxDur'). In each iteration, one of the 16 piezometers was omitted, the interpolation surface was regenerated from the remaining 15 wells using identical settings, and the predicted value was extracted at the location of the omitted piezometer.

Predictive performance was summarized using mean error (ME), mean absolute error (MAE), root mean square error (RMSE), and the Pearson correlation coefficient between observed and predicted values. ME was used to assess overall directional bias, whereas MAE and RMSE quantified the magnitude of prediction errors; both measures were retained because they emphasize different characteristics of the error distribution (Willmott and Matsuura, 2006). Detailed observed, predicted, and error values are provided in the reproducibility package.

Interpolation was constrained within the GWB 43 boundary to prevent artifacts outside the study area (e.g., Goovaerts, 1997; Hengl, 2009). We focus on metrics derived from the 12-month Standardized Groundwater Index (SGI-12) because the annual-scale aggregation emphasizes long-term groundwater drought persistence and is more closely related to prolonged hydrological impacts than shorter aggregation windows (Bloomfield and Marchant, 2013; Kumar et al., 2016).

~~We focus on metrics derived from the 12-month Standardized Groundwater Index (SGI-12) because multi-year aggregations better reflect long-term groundwater drought persistence and have stronger relationships with hydrological impacts compared to shorter windows (Bloomfield & Marchant, 2013; Kumar et al., 2016).~~

The Drought Impact Potential Index (DIPI) is defined as a weighted sum of three components: Exposure (E), Pressure (P), and Sensitivity (S). ~~Weights indicate~~The weights determine the relative ~~influence~~contribution of ~~climatic/hydrological forcing (E)~~the normalised Exposure, Pressure, and ~~human/environmental conditions (P, S) on drought impacts, following methods in compound risk assessment~~Sensitivity components to the composite DIPI score (e.g., Wheater ~~&~~and Evans, 2009; Porter et al., 2014).

All components and sub-components were ~~normalized~~normalised using min–max scaling prior to aggregation, as shown in Table 3.

Table 3: Components, sub-components, and aggregation equations of the Drought Impact Potential Index (DIPI).

Component	**Sub-component**	**Symbol**	**Definition**	**Formula**
Exposure (E)	Vulnerability	VUL′	Maximum absolute cumulative groundwater drought deficit.	$VUL' = \frac{VUL - VUL_{min}}{VUL_{max} - VUL_{min}}$
Exposure (E)	Inverse resilience	CRS_{inv}'	~~Inverted~~Inverse min-max-normalised resilience score.	$CRS_{inv}' = 1 - \frac{CRS - CRS_{min}}{CRS_{max} - CRS_{min}}$
Exposure (E)	Maximum duration	MaxDur′	Maximum duration of groundwater drought events.	$MaxDur' = \frac{MaxDur - MaxDur_{min}}{MaxDur_{max} - MaxDur_{min}}$
Exposure (E)	Composite exposure	E	Combined drought severity ~~and~~, persistence, and limited resilience.	$E = 0.4VUL' + 0.3\cancel{CRS_{inv}' +} CRS_{inv}' + 0.\cancel{3MaxDUR}3MaxDur'$
Pressure (P)	Abstraction density	Q_{dens}'	~~Groundwater~~Normalised spatial density of groundwater abstraction ~~density~~wells.	$Q_{dens}' = \frac{Q_{dens} - Q_{dens_{min}}}{Q_{dens_{max}} - Q_{dens_{min}}}$
Pressure (P)	Mining impact	Mining′	~~Mining-induced groundwater drawdown intensity~~Normalised spatial indicator of potential mining-related pressure.	—
Pressure (P)	Composite pressure	P	~~Anthropogenic stress~~Combined anthropogenic-pressure proxy.	$P = 0.7Q_{dens}' + 0.3Mining'$

Sensitivity (S)	GDE	GDE′	~~Groundwater~~ Normalised groundwater-dependent ~~ecosystems~~ecosystem indicator.	—
Sensitivity (S)	Quality	Quality′	~~Groundwater~~ Normalised groundwater-quality indicator.	—
Sensitivity (S)	Composite sensitivity	S	~~Environmental vulnerability~~Combined environmental sensitivity.	$S = 0.5GDE' + 0.5Qaulity'$
Drought Impact Potential Index		DIPI	Integrated relative drought impact ~~index~~potential.	$DIPI = 0.4E + 0.3P + 0.3S$

Notes: Variables marked with ~~(′)~~a prime (') denote ~~normalized~~dimensionless values ~~(0–1) obtained~~ normalised to the interval [0, 1] using min–max scaling~~; CRS_{inv}′ – inverted and normalized~~. CRS_{inv}' is the inverse min-max-normalised resilience ~~(1−CRS); Mining′, GDE′,~~score; higher values therefore indicate lower resilience and higher relative Exposure. Mining', GDE', and ~~Quality′~~Quality' are spatially derived indicators ~~normalized~~normalised to the range 0–1. All ~~composite indices are dimensionless. All~~ Exposure sub-components were calculated independently for each piezometer from SGI-12 metrics and interpolated separately before aggregation. The Pressure component assigns a weight of 0.7 to abstraction density and 0.3 to mining influence, whereas the two Sensitivity sub-components are equally weighted. The final DIPI uses expert-based weights of 0.4 for Exposure, 0.3 for Pressure, and 0.3 for Sensitivity. All component and composite scores are ~~first normalized to the interval [0, 1] to ensure comparability. For variables where higher values indicate lower risk (e.g., resistance/resilience), normalization is inverted,~~relative, dimensionless screening indicators and should not be interpreted as ~~shown above. The composite DIPI combines the components with the predefined weights.~~ absolute probabilities or impact magnitudes.

~~Final DIPI values are mapped using~~

The expert-based weights were used for exploratory spatial screening and were not calibrated against an independent impact dataset. The interpolated Exposure subcomponents and the independently derived Pressure and Sensitivity layers were combined to produce continuous DIPI surfaces ~~(interpolated from piezometer measurements) and~~ , which were subsequently classified into quantiles for cartographic ~~visualization.~~presentation. The full spatial representation of all ~~normalized~~normalised sub-components and both DIPI aggregation schemes is provided in Appendix A (Fig. A1) to ensure methodological transparency and reproducibility of the framework. All intermediate datasets, reproducible notebooks, and figure source tables are openly archived in Zenodo (Sawicka and Jurzyk, 2026).

~~To further disentangle the relative contributions of exposure and pressure, a~~ A spatial contrast index was ~~computed~~calculated as the difference between ~~normalized exposure~~the normalised Exposure and ~~pressure~~Pressure components (E – P). ~~This~~The index was used as a descriptive comparison of their relative mapped magnitudes and not as a causal attribution metric ~~highlights areas dominated by exposure-driven processes versus those controlled by anthropogenic pressure~~.

5. Results

5.1 Standardized Precipitation Index (SPI)

The temporal evolution of the SPI calculated for 3-, 6-, and 12-month aggregation windows reveals a largely coherent drought signal across the five precipitation stations. Although individual stations show some differences in amplitude, most drought episodes occur synchronously, indicating regionally consistent atmospheric forcing.

For SPI-3, several short and intense droughts are evident, with minima below −3 at most stations. At the 6-month scale, droughts become less abrupt but more persistent, with the most significant regional event ~~centered~~ in 2003, when the areal mean dropped to −2.93. The 12-month SPI emphasizes the multi-year nature of this episode, with the lowest areal value of −2.69 recorded in late 2003.

Overall, the mean SPI closely tracks individual stations, confirming that major drought episodes were spatially widespread rather than localized.

5.2 Standardized Groundwater Level Index (SGI)

The SGI calculated for 3-, 6-, and 12-month aggregation windows reveals ~~marked spatial differences between groundwater clusters. Although all clusters experienced periods of negative SGI, the timing and magnitude of the minima vary~~clear differences among the monitored aquifer systems in the timing, magnitude, and persistence of groundwater droughts (Fig. 4). The shallow unconfined aquifer generally showed shorter and less severe anomalies, whereas the deep confined aquifer displayed the most persistent deficits.

At the SGI-3 scale, the minimum values were −1.34 in the shallow unconfined aquifer in September 2023, −1.87 in the intermediate confined aquifer in June 2016, and −2.15 in the deep confined aquifer in September 2023. The shallow system experienced several relatively short drought episodes, including events in 2015–2016 and 2023. In the intermediate system, the most pronounced short-term event occurred in 2015–2016, followed by additional deficits in 2019–2020 and 2022–2023. In contrast, the deep aquifer showed prolonged SGI-3 droughts, including a 19-month event in 2019–2021 and a 23-month event extending from May 2022 to March 2024.

At the SGI-6 scale, the minima were −1.27, −1.72, and −2.15 for the shallow, intermediate, and deep systems, respectively. Increasing the aggregation window smoothed short-term variability and increased drought persistence, particularly in the deep aquifer. In the deep confined aquifer, one SGI-6 drought event lasted 36 months during 2019–2022, while a subsequent event lasted 22 months from June 2022 to March 2024 (Fig. 4).

~~For SGI-3, the most severe groundwater droughts happened in Cluster 2 in late 2021 (minimum −2.63) and in Cluster 3 in late 2023 (minimum −2.40). Cluster 1 experienced a shorter but clear event around 2014 (minimum −1.98). At the 6-month scale, droughts appear smoother and last longer, with Cluster 3 showing the deepest anomaly (−2.40), followed by Cluster 2 (−1.97).~~

~~SGI-12 shows a long-lasting depletion signal in Cluster 3 that stays below −2.3 into 2024 (minimum −2.39), while Clusters 1 and 2 have shallower, long-term deficits (−1.52 and −1.51, respectively).~~

~~Overall, the strongest and most persistent groundwater drought signal is consistently expressed in Cluster 3 across all aggregation windows, whereas Clusters 1 and 2 exhibit shorter or less severe episodes (Fig.4).~~

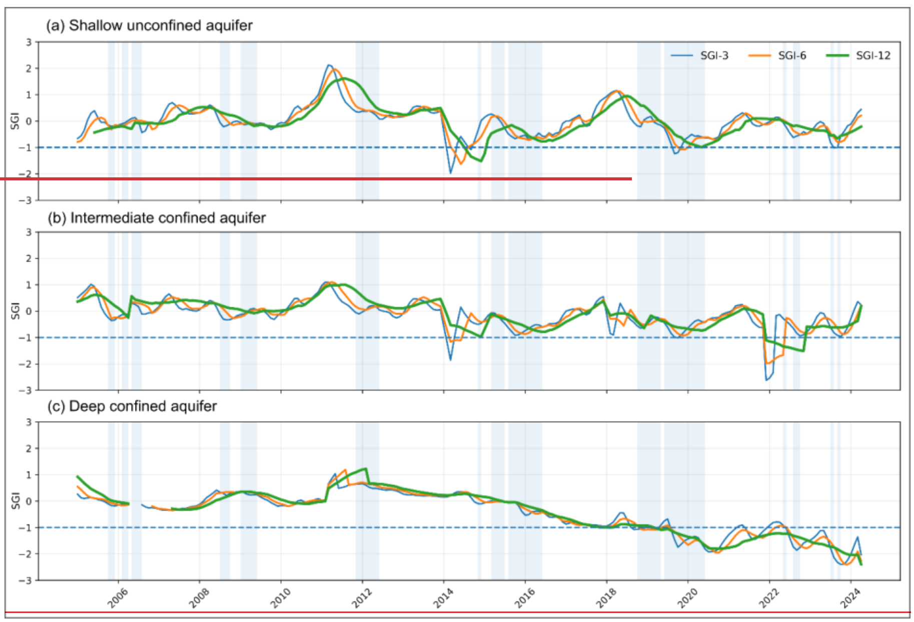

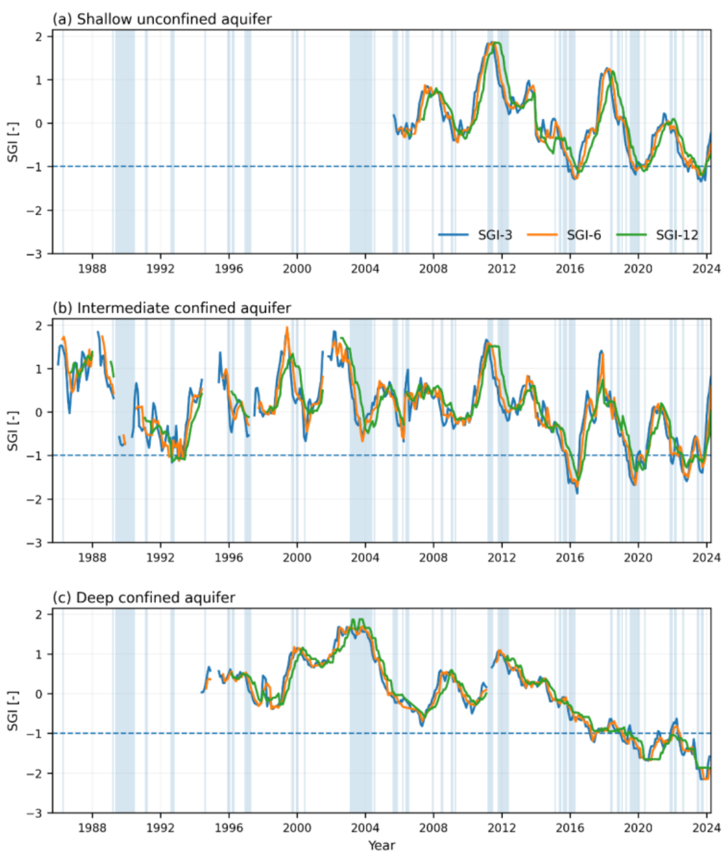

Figure 4~~:~~. Temporal ~~changes~~variation in SGI across aquifer systems and aggregation ~~levels~~timescales in GWB 43. ~~Cluster-mean~~Mean SGI-3, SGI-6, and SGI-12 time series for the three ~~groundwater~~aquifer systems~~ in GWB 43~~: (a) shallow unconfined, (b) intermediate confined, and (c) deep confined~~ aquifer~~. The dashed horizontal line ~~indicates~~marks the groundwater~~-~~–drought threshold (SGI = −1). ~~Shaded areas show periods of ~~Grey shading indicates meteorological drought ~~used for comparing with groundwater response timing and duration~~periods, defined as months in which the spatially averaged SPI-3, SPI-6, or SPI-12 was below −1.

~~To ensure comparability across aquifer systems, time series were truncated to the common observation period (2005–2024).~~

The contrast among the systems was most apparent at the SGI-12 scale. The shallow and intermediate aquifers reached minima of −1.19 and −1.57, respectively, and their drought episodes generally lasted between 5 and 10 months. In the deep confined aquifer, SGI-12 remained below −1 from August 2019 until the end of the available record in March 2024, forming a 56-month event with a minimum of −1.87. This prolonged anomaly is consistent with a persistent depletion signal in the monitored deep system, although its interpretation must account for the limited number of deep-aquifer wells and the possible influence of sustained anthropogenic pressure.

As shown in Appendix B (Fig. B1), the shallow unconfined aquifer exhibited the strongest full~~ lagged Pearson correlation matrices confirm the strongest and fastest SPI–SGI coupling in the shallow unconfined aquifer, whereas the confined systems display ~~-period SPI–SGI associations. Maximum correlations were r=0.32 for SGI-3, r=0.491 for SGI-6, and r=0.651 for SGI-12, all at a lag of 9 months.

The intermediate confined aquifer showed weaker and less uniform associations. Maximum correlations were r=0.272 at a lag of 2 months for SGI-3, r=0.325 at 5 months for SGI-6, and r=0.281 at 6 months for SGI-12.

In the deep confined aquifer, maximum correlations were r=0.184, r=0.303, and r=0.380 for SGI-3, SGI-6, and SGI-12, respectively. All maxima occurred at the upper tested lag of 12 months, indicating that the strongest association may occur beyond the analysed range and cannot be resolved precisely.

Overall, the full-period results are consistent with the strongest and most coherent meteorological association in the shallow unconfined aquifer and a progressively delayed ~~responses~~relationship in the deep confined aquifer. However, the moving-window analysis showed that the lag associated with the maximum correlation varied among subperiods (Appendix C, Fig. C1). The reported lags should therefore be interpreted as empirical indicators of temporal association within the tested range rather than as fixed aquifer-response times or direct evidence of a propagation mechanism.

The moving-window analysis showed that the lag associated with the maximum SPI–SGI correlation was not fully stationary through time (Appendix C, Fig. C1). In the shallow unconfined aquifer, the SGI-12 maximum was comparatively stable and generally occurred at lags of 7–10 months, most frequently at 9 months. The intermediate confined aquifer showed relatively stable maxima for SGI-6 and SGI-12, whereas the SGI-3 lag varied more strongly among subperiods. In the deep confined aquifer, maximum correlations most frequently occurred near the upper boundary of the tested range, particularly for SGI-6 and SGI-12.

5.3 Drought metrics

Groundwater drought characteristics derived from the SGI ~~reveal distinct~~series show clear differences ~~between clusters~~among aquifer groups and ~~scales of~~ aggregation ~~(Tab.~~scales (Table 4; Fig. 5). At ~~SGI-~~the 3~~, droughts tend to be frequent but short. Cluster 1~~-month scale, drought events were shortest in the shallow and intermediate aquifers. The shallow unconfined aquifer experienced ~~four~~five events with ~~an average~~a mean duration of ~~2~~4.0 months and a maximum duration of ~~3~~7 months, ~~while~~

~~Cluster 2 shows greater severity (−3.93). Cluster 3 has longer events, averaging 11 months with a maximum of 23 months, and a mean severity of −17.07.~~

~~At SGI-6, events become fewer and longer. Cluster 2~~whereas the intermediate confined aquifer experienced ~~four~~eight events ~~(average~~with a mean duration of 4~~5~~.1 months~~;~~ and a maximum duration of ~~6~~10 months~~), while Cluster 1 had shorter events. Cluster 3 shows~~. The deep confined aquifer showed substantially longer and more ~~persistent droughts.~~

~~At SGI-12, droughts are primarily characterized by multi-year events. Cluster 3 features two events lasting over 50 months with the highest severity (−45.83). Clusters 1 and 2 experience shorter, less~~ severe droughts, with a mean duration of 11.8 months, a maximum duration of 23 months, and a mean cumulative severity of −16.96.

At the 6-month scale, droughts in the shallow unconfined and intermediate confined aquifers remained comparatively short, with mean durations of 3.3 and 4.2 months, respectively. In contrast, the deep confined aquifer experienced only three events, but their mean duration increased to 20.7 months, and the longest event lasted 36 months. The corresponding vulnerability value (VUL) increased to 47.02, compared with 8.87 and 13.38 in the shallow unconfined and intermediate confined aquifers.

At the 12-month scale, the contrast between the deep aquifer and the two shallower systems remained pronounced. The shallow unconfined aquifer experienced four events with a mean duration of 4.3 months, whereas the intermediate confined aquifer experienced five events with a mean duration of 8.8 months. The deep confined aquifer experienced two long-term events with a mean duration of 29 months and a maximum duration of 56 months. It also had the highest cumulative severity (−41.09) and vulnerability (VUL = 80.10).

Resistance (CRT), defined as the fraction of valid months outside groundwater drought, ranged from 0.815 to 0.918. The lowest values occurred in the deep confined aquifer, indicating a larger proportion of months affected by drought. Resilience (CRS), defined as the probability of transition from drought to non-drought conditions, was also lowest in the deep confined aquifer and declined from 0.069 at SGI-3 to 0.018 at SGI-12.

Recovery was observed for all SGI-3 and SGI-6 events in shallow and intermediate aquifers. Median recovery times ranged from 4 to 12 months. At SGI-12, two of four events in the shallow unconfined aquifer recovered, with a median recovery time of 10.5 months, whereas all five events in the intermediate confined aquifer recovered within a median of 12 months. No recovery was observed for any event in the deep confined aquifer within the available observation period.

Across the monitored aquifer systems, the deep confined aquifer exhibited the longest and most persistent drought episodes. Because it is represented by only two wells, this contrast should be interpreted as characteristic of the monitored locations rather than as a general depth-dependent relationship.

Table 4~~:~~. Groundwater drought metrics ~~across~~derived from aquifer~~ systems~~-group mean SGI series at 3-, 6-, and ~~SGI~~12-month aggregation scales~~ in GWB 43. Abbreviations: VUL – vulnerability; CRT – resistance; CRS – resilience~~.

SGI scale	~~Cluster~~Aquife	N	Mean ~~dur.~~duration	Max ~~dur.~~duration	Mean ~~sev.~~s	~~Prop.~~Propaga	~~Recovery~~Media	Reco	Unrecovered events	CRT	CRS	VUL

Wstawione komórki

Wstawione komórki

	r system				(months)	(months)	severity	tion SGI-3→SGI-12	n recovery (months)	vered events					
SGI-3	1			5	4.0	~~2~~7.0	~~3-~~4.7	- ~~2.6~~1.00	~~0.25~~1 2.00	~~7~~5		0	0.~~9~~ ~~0~~91	0.~~0~~ ~~9~~25	~~12.~~ ~~7~~8.67
SGI-3	2	~~2~~ 8	~~3~~		5.1	10.0	-6.9	1.00	~~-~~4.400	8	0.~~14~~	~~11~~	0.9 0	0.~~1~~ ~~1~~19	~~22.~~ ~~2~~15.18
SGI-3	3	~~1~~ 5	~~6~~	~~6~~	- 11.8~~.2~~	23.0	~~0.~~- 17.0	~~32~~0.80	n.r.	0		5	0.~~9~~ ~~5~~83	0.~~0~~ ~~5~~07	~~118~~ ~~.1~~37.69
SGI-6	1	~~5~~ 6	~~2~~		3.3	8.0	-3.~~9~~7	~~0.31~~ —	10.50	6		0	0.9 1	0.~~0~~ ~~9~~30	~~13.~~ ~~5~~8.87
SGI-6	2			~~4~~9	4.2	~~6~~9.0	-5.~~6~~4	~~0.44~~ —	~~17~~6.0 0	~~0.94~~ 9		0.~~07~~	0.9 1	0.2 4.~~3~~	13.38
SGI-6	3			~~2~~3	20.7	~~12~~36.0	- ~~9~~29.2	~~0.07~~ —	n.r.~~31~~	0.~~97~~		3	0.8 1	0.0 3	~~122~~ ~~.6~~47.02
SGI-12	1			~~5~~4	~~11~~4.3	~~23~~6.0	- ~~17.1~~ 4.6	~~0.40~~ —	10.50* ~~n.r.~~	~~0.96~~ 2		~~0.03~~2	~~25.~~ ~~3~~0.92	0.2 3	6.4 7
SGI-12	2			~~3~~5	~~20~~8.8	~~31~~10.0	- ~~30.5~~ 10.4	~~0.47~~ —	12.00~~n.r.~~	~~0.96~~ 5		0.~~06~~	~~25.~~ ~~2~~0.88	0.1 1	12.83

Wstawione komórki
Usunięte komórki
Usunięte komórki
Wstawione komórki
Wstawione komórki
Wstawione komórki
Wstawione komórki
Usunięte komórki
Wstawione komórki
Wstawione komórki
Wstawione komórki
Wstawione komórki
Wstawione komórki
Wstawione komórki
Wstawione komórki

SGI-12	3	2	~~31~~29.0	~~61~~56.0	- ~~47.0~~ 41.1	~~0.48~~ —	n.r.	0~~.98~~	~~0.03~~2	~~12~~ ~~2.4~~ 0.81	0.02	80.10

~~n.r. – no recovery observed within the observation period.~~

~~Resilience decreases as SGI aggregation windows lengthen, while resistance rises. Cluster 3 shows consistently high vulnerability across all SGI scales, with low resilience. Resistance increases with longer SGI aggregation, indicating the cumulative buffering capacity of groundwater systems. Median recovery also grows with aggregation scale and reaches 'no recovery' (n.r.) at SGI-12 for all clusters (Fig.5c).~~

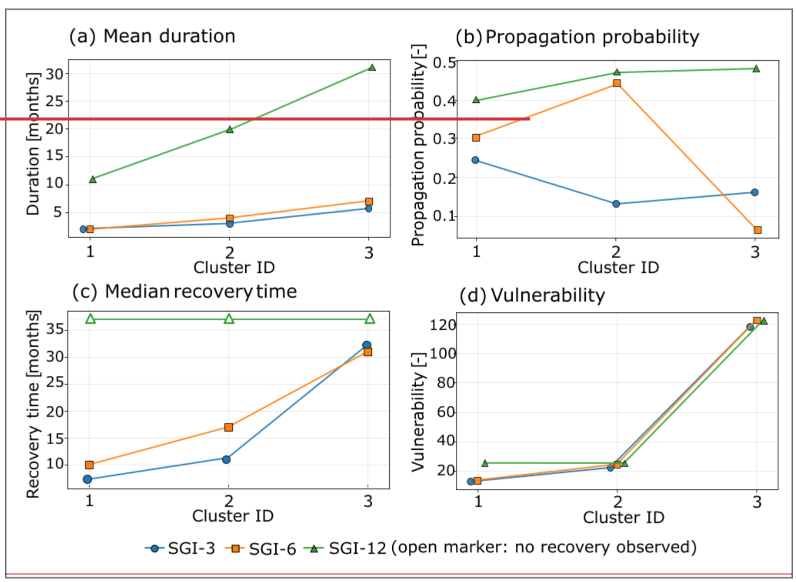

~~**Figure 5:** Groundwater drought metrics across aquifer systems and timescales. Comparison of drought metrics derived from SGI-3, SGI-6, and SGI-12 for the three aquifer systems in GWB 43: (a) mean drought duration, (b) propagation likelihood, (c) median recovery time, and (d) vulnerability (VUL). Open markers in panel (c) indicate cases where recovery to near-normal conditions (SGI ≥ −0.5) was not observed within the study period.~~

Notes: Propagation probability is defined only for the transition from SGI-3 to SGI-12 and is therefore reported in the SGI-3 rows. Recovery denotes the median number of months from the event minimum to the first month with SGI ≥ −0.5. CRT is the fraction of valid months outside drought conditions, whereas CRS is the one-step probability of transition from drought to non-drought. VUL is the maximum absolute cumulative SGI deficit across drought events. Recovered and unrecovered events indicate the number of events for which recovery was or was not observed. Mean severity is expressed as the signed mean cumulative SGI severity; negative values indicate groundwater deficit. Propagation probability denotes the fraction of SGI-3 events matched to an SGI-12 event. For the shallow unconfined aquifer at SGI-12, the median recovery time of 10.5 months is based on two recovered events; two additional events did not recover within the available record. n.r. – no recovery observed; — not applicable.

Figure 5 shows systematic differences in drought patterns across groundwater systems. Duration and vulnerability ~~rise sharply with system depth, while propagation probability follows non-linear trends, especially in the deep confined system. Recovery time increases with aggregation scale and becomes nearly unbounded at SGI-12, indicating ongoing drought conditions~~were highest in the monitored deep confined aquifer, whereas propagation probability showed less systematic variation among aquifer systems. At SGI-12, recovery time could not be estimated for the deep confined aquifer because no recovery was observed within the available record.

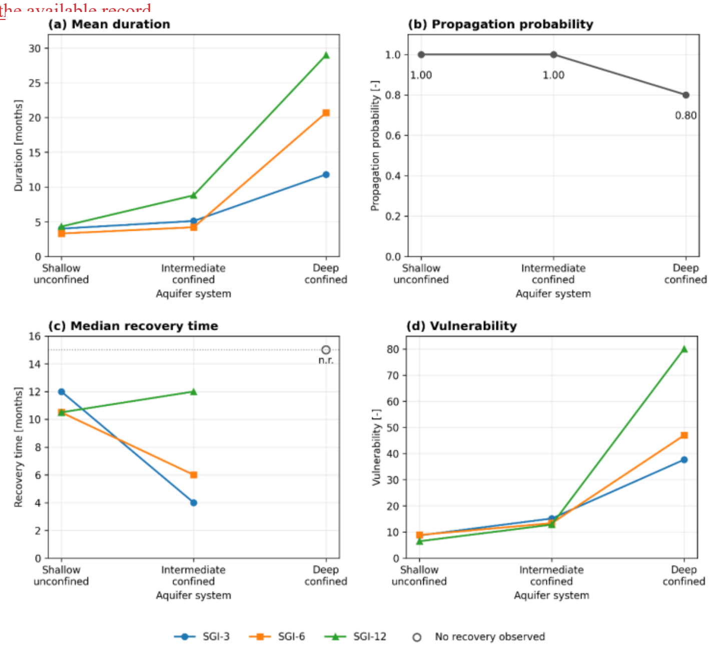

~~Propagation probability increases with aggregation scale. At short timescales (SGI-3), propagation remains limited across all clusters, whereas at longer timescales (SGI-12) it becomes substantial, particularly in Clusters 2 and 3 (Fig.6).~~

~~Clear differences appear among the clusters. Cluster 1 shows low propagation probability and quick response, suggesting a system closely linked to short-term recharge. Cluster 2 demonstrates intermediate behavior, where propagation only becomes significant at seasonal to annual scales. Meanwhile, Cluster 3 exhibits delayed but ultimately strong propagation, matching a system with long memory and cumulative storage effects.~~

~~Recovery times increase substantially with the aggregation scale and differ substantially across clusters. Cluster 1 recovers rapidly after drought events, typically within a few months, indicating high system resilience. Cluster 2 exhibits delayed recovery, suggesting partial storage depletion during consecutive dry periods. In Cluster 3, recovery is extremely limited, with groundwater levels often failing to return to near-normal conditions within the observation period.~~

~~These dynamics are reflected in the performance metrics: increasing resistance (CRT) and decreasing resilience (CRS) with longer aggregation scales, together with high vulnerability (VUL) in Cluster 3, confirm that groundwater systems become progressively less capable of recovering from prolonged deficits.~~

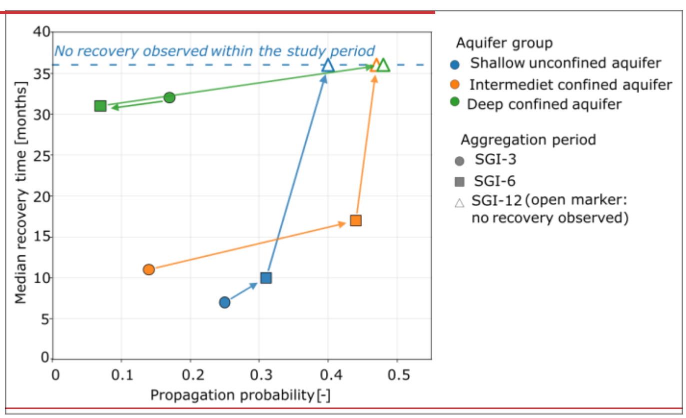

~~**Figure 6:** Groundwater drought propagation–recovery trajectories across aquifer systems. Shows the relationship between groundwater drought propagation probability and median recovery time for shallow, intermediate, and deep aquifers in GWB 43. Marker shape indicates the temporal aggregation scale (SGI-3, SGI-6, SGI-12), while arrows depict the system's response trajectory as temporal integration increases. Open markers at the upper reference line signify no observed recovery within the common observation period.~~

~~Figure 6 highlights contrasting propagation recovery behavior among aquifer systems. In the shallow and intermediate systems, the probability of propagation increases with aggregation scale, along with longer recovery times. In contrast, the~~

~~deep confined system shows non-monotonic behavior, with a decrease in propagation from SGI-3 to SGI-6, followed by an increase at SGI-12. This reflects temporal filtering of short-term deficits and a threshold-type response to prolonged forcing.~~ ~~In the deep confined system, propagation probability decreases from SGI-3 to SGI-6, indicating that short-term groundwater anomalies do not translate into sustained seasonal-scale drought. This reflects temporal filtering of recharge deficits and suggests a minimum duration threshold for drought propagation in the deep aquifer.~~

Figure 5. Groundwater drought metrics across the three monitored aquifer systems and aggregation scales. Comparison of (a) mean drought duration, (b) propagation probability from SGI-3 to SGI-12, (c) median recovery time, and (d) vulnerability (VUL) for the shallow unconfined, intermediate confined, and deep confined aquifer systems. Mean duration, recovery time, and vulnerability are shown for SGI-3, SGI-6, and SGI-12. Propagation probability is reported as a single SGI-3-to-SGI-12 value for each aquifer system. Open symbols and "n.r." indicate that no recovery was observed within the available monitoring period.

5.4 Groundwater drought propagation and recovery

Propagation probability was defined as the fraction of SGI-3 drought events matched to an overlapping SGI-12 event or to a subsequent SGI-12 event beginning within 12 months of the SGI-3 event onset. Each SGI-3 event was counted only once. Under this definition, all SGI-3 events in the shallow unconfined and intermediate confined aquifers propagated to the 12-month scale, giving propagation probabilities of 1.00. In the deep confined aquifer, four of five SGI-3 events were matched to SGI-12 events, resulting in a propagation probability of 0.80.

These values are consistent with a short-term groundwater drought being commonly associated with a longer-term groundwater deficit in all three aquifer systems. However, propagation probability alone did not distinguish the deep aquifer as the most drought-prone system. The strongest contrast among aquifer groups was instead expressed by drought duration, cumulative severity, vulnerability, and recovery behaviour.

The shallow and intermediate aquifers generally showed shorter drought events and more frequent recovery. All SGI-3 and SGI-6 events in the shallow unconfined and intermediate confined aquifers returned to near-normal conditions within the available record. At SGI-12, recovery was observed for all events in the intermediate confined aquifer, whereas two of four events in the shallow unconfined aquifer did not recover before the end of the available series.

The deep confined aquifer displayed a markedly different response. Its drought events were longer and more severe at all aggregation scales, and no event recovered to SGI ≥ -0.5 within the available observation period. The progressive decrease in CRS and the increase in maximum duration and VUL with aggregation scale are consistent with persistent groundwater deficits and limited short-term recovery.

Because aquifer depth is confounded with geographic location, monitoring-period length, and hydrogeological setting, these differences should not be interpreted as a general depth-dependent relationship. They describe the behaviour of the monitored aquifer groups within GWB 43 and should be viewed as characteristic of these specific hydrogeological settings.

Piezometer-level propagation probabilities ranged from approximately 0.57 to 1.00, indicating substantial within-aquifer-system variability (Fig. 6). These values were calculated independently for individual piezometers and therefore should not be interpreted as deviations around the aquifer-system-level probabilities derived from aquifer-group mean SGI series.

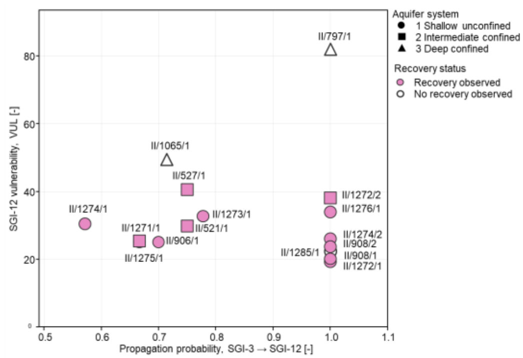

Figure 6. Piezometer-level relationship between groundwater drought propagation and long-term persistence. Propagation probability was calculated independently for each piezometer as the fraction of SGI-3 drought events matched to an overlapping SGI-12 event or to a subsequent SGI-12 event beginning within 12 months of the SGI-3 event onset. Each SGI-3 event was counted only once. The vertical axis shows piezometer-level SGI-12 vulnerability (VUL), while marker size represents the maximum SGI-12 drought duration. Marker shape identifies the aquifer system, pink-filled symbols indicate that recovery to SGI ≥ −0.5 was observed for at least one event, and open symbols indicate no observed recovery within the available record.

5.5. Drought Impact Potential Index (DIPI)

~~To evaluate~~The mapped DIPI values represent relative spatial scores within GWB 43 and should not be interpreted as absolute probabilities or magnitudes of groundwater drought impact. The revised DIPI was calculated as a weighted combination of Exposure, Pressure, and Sensitivity: DIPI = 0.4E + 0.3P + 0.3S.

An equally weighted formulation (DIPI = (E+P+S)/3) was also calculated to examine the sensitivity of the ~~DIPI formulation~~ spatial pattern to the ~~weighting scheme, both a weighted (0.4E + 0.3P + 0.3S) and an unweighted (E + P + S)/3 approach were applied. The strong spatial agreement between the equal-weight and weighted DIPI variants (~~adopted component weights.

The weighted and equally weighted formulations produced broadly similar regional patterns, with areas of comparatively higher and lower index values occurring in similar parts of the study area (Fig. 7; Appendix A, Fig. ~~A1 f, i) confirms~~A1). Differences between the two formulations were mainly expressed as local changes in index magnitude and class boundaries.

The comparison is consistent with the idea that the ~~identified hotspot configuration is~~ broad spatial pattern was similar under the two tested weighting schemes. However, it should not be interpreted as evidence that individual mapped values or the boundaries of higher-index areas are spatially robust ~~to the aggregation scheme~~.

The ~~resulting maps exhibit a highly consistent spatial pattern, with the main high-index zones preserved in both cases. In particular, a coherent high-~~ weighted DIPI ~~area is observed~~ranged from approximately 0.066 to 0.583. Comparatively higher values occurred mainly in the central and ~~southern~~east-central parts of ~~the groundwater body~~GWB 43, whereas lower values ~~predominate~~were more common in the northern sector ~~(Fig. 7).~~

~~Differences between the two formulations are limited to minor variations in class boundaries~~ and ~~local intensity, without affecting the overall spatial configuration of hotspots. This indicates that the DIPI pattern is robust with respect to the assumed weighting scheme.~~in parts of the southern area. The ~~spatial configuration of high- and low-value areas remains largely unchanged between panels, indicating a stable~~ resulting surface reflects the combined spatial distribution of ~~index values. Variations between panels are limited to minor changes in intensity and class boundaries~~groundwater drought Exposure, anthropogenic Pressure, and environmental Sensitivity. It should therefore be interpreted as an exploratory screening representation of relative drought impact potential rather than as a predictive vulnerability map.

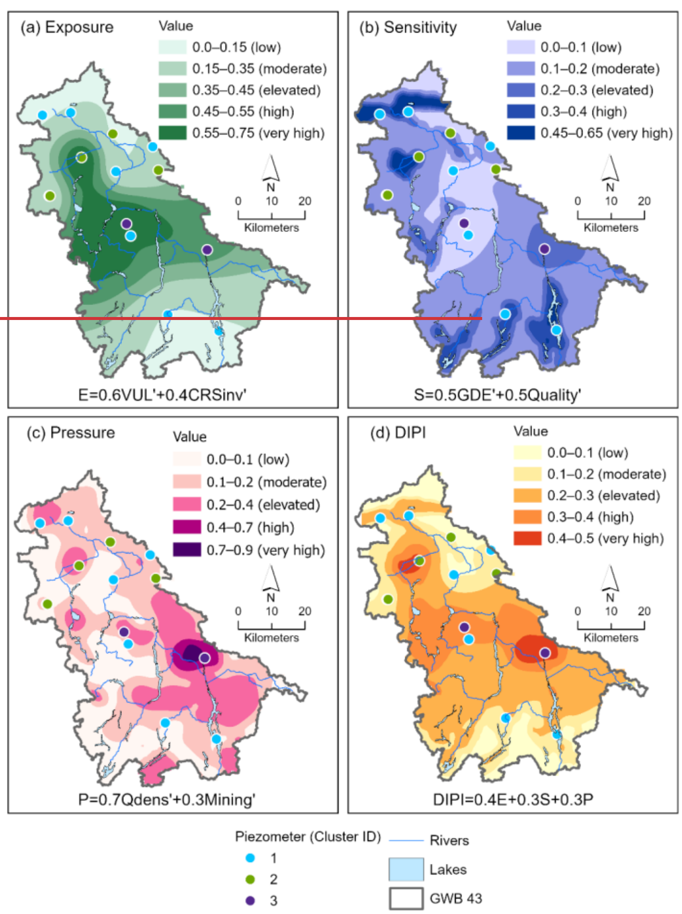

Aggregation of DIPI values at piezometer locations showed very similar mean scores for the shallow unconfined and intermediate confined aquifer systems. Under the weighted formulation, mean DIPI was 0.187 for the shallow unconfined aquifer and 0.189 for the intermediate confined aquifer, while the deep confined aquifer reached 0.470. The equal-weight formulation produced corresponding values of 0.194, 0.182, and 0.442. Thus, the distinction between the shallow and intermediate aquifer systems is limited, whereas the deep confined aquifer consistently shows substantially higher relative

DIPI values under both weighting schemes. Because the deep confined aquifer is represented by only two piezometers, this contrast should be interpreted cautiously and as indicative rather than spatially representative.

Leave-one-out cross-validation of the three interpolated Exposure subcomponents indicated substantial spatial uncertainty. Across normalised vulnerability, inverse resilience, and maximum drought duration, MAE ranged from 0.211 to 0.287 and RMSE from 0.315 to 0.344. Mean errors were close to zero, indicating limited overall bias, but observed–predicted correlations were weak (r=−0.195 to 0.108). The largest errors occurred in sparsely monitored areas and where spatially adjacent piezometers represented different aquifer systems with contrasting drought-response metrics. These results are consistent with limited ability to reproduce local piezometer-scale variability and support interpreting the DIPI surface as an exploratory regional screening product.

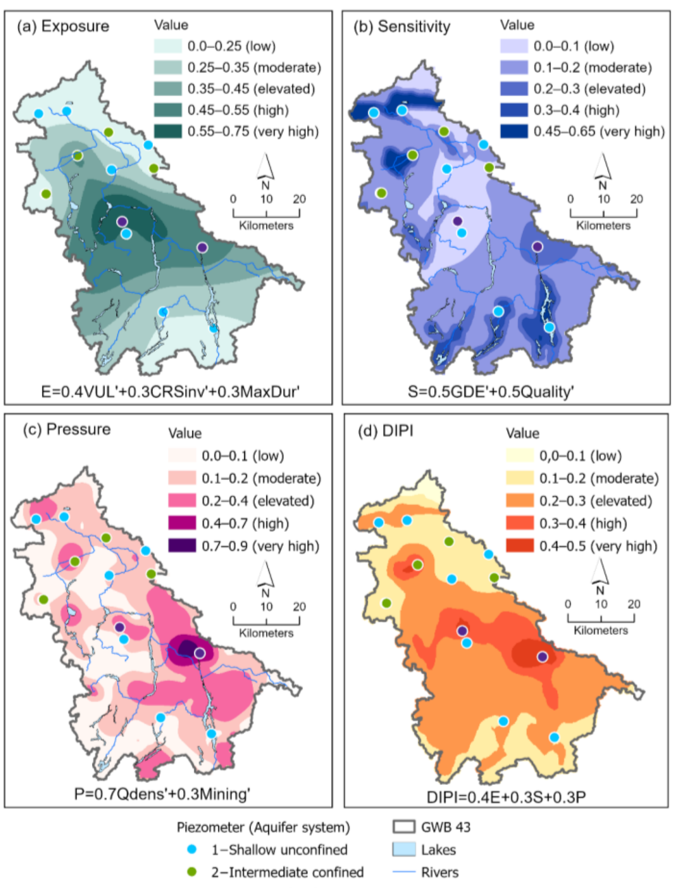

Figure 7: Spatial distribution of DIPI and its component layers in GWB 43. Spatial distribution of the Drought Impact Potential Index (DIPI) and its component layers: (a) Exposure (E), (b) Sensitivity (S), (c) Pressure (P), and (d) final DIPI. Exposure integrates~~ process-based~~ groundwater drought metrics, sensitivity reflects GDE and groundwater-quality constraints, and pressure represents abstraction~~–~~-density and mining-~~related stress.~~influence proxies. All components were ~~normalized~~normalised to the 0–1 range prior to integration.

~~Aggregation of DIPI at the cluster level showed a clear increase from shallow unconfined aquifers (0.195) to intermediate confined systems (0.219), with the highest average value found in deep confined aquifers (0.407). This pattern suggests that the increased drought impact potential in deeper aquifer systems is mainly driven by greater exposure rather than significant differences in sensitivity.~~

5.6. Exposure–pressure contrast

The spatial contrast between ~~normalized exposure~~normalised Exposure (E) and ~~pressure~~Pressure (P~~) components within GWB 43,~~), expressed as E~~ – ~~−P, ~~shows mostly~~was predominantly positive ~~values ~~across ~~the study area~~GWB 43, with ~~some ~~localized ~~zones of~~ negative ~~values. ~~and near-zero zones (Fig. 8). Positive values ~~suggest ~~are consistent with areas where ~~drought impact potential is mainly driven by the natural groundwater system response, while~~the mapped Exposure score exceeds the mapped Pressure score, negative values ~~indicate zones dominated by human activities. Near-zero values~~are consistent with the opposite, and values between −0.1 and 0.1 represent a balanced ~~conditions where both components contribute equally (Fig. 8). The map shows that most areas are exposure-driven, with pressure-dominated zones limited to small patches.~~contrast. Area-based classification showed that E>P covered 65.5% of the study area, E≈P covered 31.6%, and E<P covered 2.9%. These classes describe only the relative mapped magnitudes of the ~~exposure–pressure contrast (E − P) reveals that exposure-dominated zones make up 60.4% of GWB 43, pressure-dominated areas account for 21.8%, and balanced conditions, where both components are similar, cover 17.8% of the study area.~~

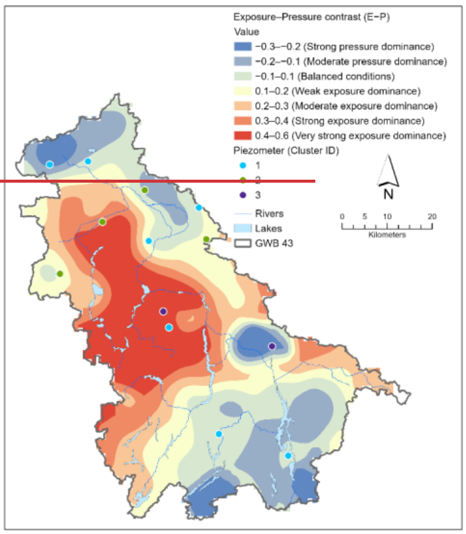

two normalised components and do not provide causal attribution of groundwater-

~~**Figure 8**~~: ~~Exposure–pressure contrast map of groundwater~~ drought controls ~~in GWB 43.~~(Fig. 8).

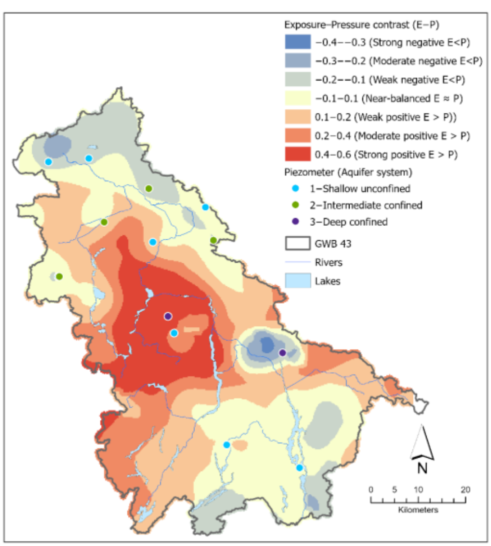

Figure 8

. Spatial contrast between ~~normalized~~normalised Exposure (E) and Pressure (P) in GWB 43. Positive values are consistent with areas where E exceeds P, negative values are consistent with areas where P exceeds E, and values between −0.1 and 0.1 represent a balanced contrast. The E−P classes provide a descriptive comparison of the relative mapped component magnitudes and should not be interpreted as causal attribution.

Spatial contrast between normalised Exposure (E) and Pressure (P) is expressed as E − P. Positive values ~~indicate~~are consistent with areas ~~dominated by the natural aquifer-system response, while negative values highlight zones~~ where ~~human activity has a greater influence on groundwater drought impact.~~the normalised Exposure score exceeds the normalised Pressure score, whereas negative values are consistent with areas where Pressure exceeds Exposure. Values close to zero ~~suggest a balanced effect of both factors~~are consistent with similar mapped magnitudes of the two components. The contrast is descriptive and does not separate natural and anthropogenic controls.

6. Discussion

The combined analysis of SGI time series, propagation–recovery relationships, and ~~aggregated~~ drought metrics ~~reveals a clear system-dependent control on groundwater drought behavior~~ is consistent with contrasting temporal behaviour among the monitored aquifer systems in GWB 43. ~~Shallow~~The shallow unconfined ~~systems respond rapidly to meteorological forcing, with high propagation efficiency~~system generally exhibits shorter and ~~relatively fast recovery, reflecting limited storage and low system memory. In contrast,~~ less persistent groundwater deficits, whereas the intermediate ~~systems exhibit attenuated and delayed responses, indicating partial decoupling from short-term recharge variability. The~~ and deep confined ~~system shows fundamentally different dynamics, characterized~~systems show increasingly prolonged anomalies. The persistent signal in the deep aquifer is consistent with greater system memory, although its interpretation remains constrained by ~~non-linear propagation, threshold-type response, and extremely long or absent recovery~~the limited number of monitoring wells and the possible influence of sustained anthropogenic pressure.

These results integrate groundwater drought into a ~~process-based~~hydrogeologically informed statistical framework~~, where the~~ in which observed system ~~response is driven by the interaction~~behaviour reflects interactions between external ~~forces~~forcing and ~~internal~~ aquifer characteristics, consistent with recent large-sample groundwater studies (Ebeling et al., 2025).

6.1 System memory and aquifer depth

~~The results show that groundwater drought behavior is strongly influenced by system memory, which systematically varies with aquifer depth and hydrogeological structure. Shallow systems respond quickly to short-term changes in recharge,~~

~~experiencing frequent but temporary drought episodes. Conversely, deeper systems have delayed responses, longer drought durations, and persistent water deficits, reflecting the cumulative effect of recharge over extended periods.~~

The observed contrasts are consistent with differences in aquifer memory associated with confinement, storage, and recharge connectivity. The stronger SPI–SGI association in the shallow unconfined aquifer suggests lower attenuation of precipitation variability and closer hydraulic connection with recharge. In the confined systems, greater storage and hydraulic separation may attenuate short-term variability and prolong groundwater-level anomalies. However, these patterns cannot be attributed solely to aquifer depth because monitoring location, record length, hydraulic connectivity, and anthropogenic modification differ among the groups.

This ~~behavior~~behaviour aligns with previous research emphasizing the importance of aquifer storage and hydraulic connectivity in regulating groundwater memory (Van Loon, 2015; Bloomfield ~~&~~and Marchant, 2013). Recent studies further verify that groundwater response times and memory are heavily influenced by aquifer depth and hydrogeological conditions (Ebeling et al., 2025).

Furthermore, recent studies of the land water cycle show that hydrological memory greatly increases from atmospheric to underground parts, with groundwater showing the strongest persistence and long-term storage effects (Berghuijs et al., 2025). As a result, deeper and more confined systems display smoother but more persistent drought signals, while shallow systems maintain closer connection with atmospheric forcing. These findings ~~confirm~~support the interpretation that groundwater drought cannot be viewed simply as a reaction to precipitation anomalies, but must be understood as influenced by aquifer structure and internal system dynamics.

6.2 Propagation and recovery asymmetry

~~A key finding of this study is the clear imbalance~~The results indicate an asymmetry between drought ~~propagation~~development and recovery~~ processes. While propagation happens when ~~. Propagation is associated with the accumulation of meteorological deficits~~ build up enough to decrease recharge,~~, whereas recovery depends on sustained recharge and ~~often extended recharge input, making it inherently slower~~restoration of groundwater storage. In the monitored deep confined aquifer, drought events were less frequent but more persistent, while the shallow unconfined aquifer generally showed shorter deficits and more ~~limited~~frequent recovery.

This asymmetry is especially clear in deeper systems, where droughts happen less often but, once they start, last longer and recover slowly. In contrast, shallow systems show both quick spread and quick recovery, reflecting a more active but less lasting response pattern.

Recent studies increasingly emphasize that drought propagation and recovery are governed by fundamentally different mechanisms: propagation by cumulative deficits and recovery by recharge conditions and storage dynamics (Van Loon et al., 2016; Barker et al., 2016; Jasechko, 2026).

This decoupling explains why groundwater drought persists even after meteorological conditions improve and points out the limitations of interpreting groundwater drought only through climatic indices.

~~The substantial share of pressure-dominated areas (21.8%) indicates that anthropogenic forcing exerts a spatially significant control on groundwater drought impact in GWB 43, yet the predominance of exposure-driven zones confirms that intrinsic system properties remain the primary factor governing drought persistence and spatial variability.~~

~~Notably, pressure-dominated zones mainly align with areas affected by mining-related dewatering, indicating that human-induced drawdown locally intensifies groundwater drought signals, while the larger spatial pattern remains driven by aquifer-scale storage and recovery processes.~~

6.3 Process-~~based~~informed interpretation of the DIPI framework

~~The cluster-level DIPI gradient supports the interpretation that aquifer architecture exerts a first-order control on drought impact potential. The substantially higher DIPI in deep confined systems suggests that prolonged event duration and larger cumulative severity outweigh their only moderately different sensitivity, leading to a markedly stronger integrated drought-risk signal. The stability of the DIPI spatial pattern across various weighting schemes shows that the index reflects inherent properties of the groundwater system rather than model configuration artifacts. The agreement between weighted and unweighted versions indicates that the relative roles of exposure, pressure, and sensitivity do not change the core spatial structure of drought impact potential.~~

The DIPI integrates spatially interpolated Exposure, Pressure, and Sensitivity components into an exploratory representation of groundwater drought impact potential. The Exposure component incorporates SGI-12 drought-response metrics derived from observed groundwater-level behaviour, while Pressure and Sensitivity are represented by spatial proxy indicators. The resulting index therefore extends beyond a purely static assessment by incorporating information on the observed duration, vulnerability, and recovery characteristics of groundwater drought.

At the same time, DIPI should be interpreted as a screening framework rather than as a predictive or causally resolved vulnerability model. The monitoring network is limited, particularly for the deep confined system, and spatial interpolation introduces uncertainty in areas distant from observation wells. The Pressure component also has important limitations: well density does not directly quantify abstraction volumes, and the mining layer delineates zones of potential influence without representing temporal variability or dewatering intensity. Moreover, Exposure and Pressure are not fully independent because the observed groundwater-level records used to calculate SGI may already reflect anthropogenic effects.

The spatial pattern represents the combined mapped influence of groundwater drought behaviour, anthropogenic-pressure proxies, and environmental sensitivity. Areas with higher DIPI values should therefore be interpreted as locations where these normalised components jointly produce comparatively higher index scores, rather than as confirmed groundwater drought hotspots or direct evidence of a particular controlling process. Similarly, differences among aquifer systems are consistent with contrasts in drought persistence and system memory, but they cannot be attributed solely to aquifer architecture because climatic forcing, hydraulic connectivity, monitoring configuration, and anthropogenic pressure may contribute simultaneously.

The component weights remain expert-based and require external calibration and validation. The comparison between weighted and equally weighted formulations is consistent with sensitivity to the adopted weighting structure, but it does not establish the robustness of the detailed spatial pattern. Consequently, agreement between alternative formulations should be interpreted as supporting the general framework structure rather than confirming individual mapped values or hotspot boundaries.

Unlike ~~traditional~~conventional vulnerability indices ~~that rely on static indicators or expert judgment, the exposure component specifically includes process-~~based entirely on static hydrogeological attributes, DIPI incorporates hydrogeologically informed drought-response metrics ~~that connect spatial patterns to groundwater system dynamics~~into the Exposure component. This ~~method aligns~~is consistent with recent ~~advances in drought~~ research emphasizing ~~dynamic~~the importance of temporal system ~~responses and process-based understanding of~~ behaviour in drought ~~phenomena~~assessment (Kumar et al., 2020; Vega Briones et al., 2024; Kartal ~~&~~and Nones, 2024).

~~DIPI reflects a~~ The framework thus provides a structured synthesis of observed ~~system responses rather than a purely statistical aggregation. Spatial patterns thus emerge from the interaction between external forcing and internal system properties, offering a physically grounded interpretation of groundwater drought vulnerability~~groundwater behaviour and spatial indicators, while its outputs remain exploratory and dependent on the quality, density, and representativeness of the available data.

6.4 Anthropogenic pressure and mining effects

Anthropogenic pressure, ~~especially~~particularly mining-related dewatering, ~~adds an extra influence on~~may modify groundwater drought dynamics by altering hydraulic gradients~~ and~~, groundwater storage, and background water-level conditions. Long-term drainage ~~from~~associated with open-pit mining ~~lowers~~can lower groundwater levels and ~~can~~potentially intensify the ~~impacts~~effects of meteorological deficits, ~~effectively decreasing~~thereby increasing the ~~threshold for~~likelihood and persistence of groundwater drought ~~initiation~~conditions.

Recent studies increasingly distinguish between climate-driven and human-modified groundwater drought, ~~highlighting~~emphasizing that anthropogenic pressures may ~~significantly~~ alter ~~natural system~~aquifer response and drought persistence (Vega Briones et al., 2024; Jasechko~~ et al.,~~, 2026). In such settings, the distinction between meteorological-drought propagation and anthropogenically induced drawdown becomes difficult to resolve because both influences are recorded within the same groundwater-level series. Their combined effects may contribute to prolonged deficits and delayed recovery, particularly in deeper or hydraulically connected aquifers.

~~In such systems, the distinction between natural drought and anthropogenically induced drawdown becomes less clear, as both processes interact within the same hydraulic framework. This interaction may enhance drought persistence and delay recovery, especially in deeper or hydraulically connected aquifers.~~

~~The results show that mining-induced drawdown amplifies drought conditions locally, while the overall spatial pattern is governed by aquifer-scale processes.~~

In the multilayered GWB 43 system, dewatering of deeper horizons may alter vertical hydraulic gradients and induce downward leakage from shallower aquifers toward the drained zones. Consequently, groundwater-level declines recorded in shallow piezometers may reflect not only precipitation-deficit propagation and local abstraction but also hydraulic redistribution associated with mining. Quantitative separation of these mechanisms would require nested or paired shallow and deep piezometers at the same locations, which are not available in the present monitoring network.

The mapped E−P contrast was positive across 65.5% of GWB 43, near-balanced across 31.6%, and negative across 2.9% (Fig 8). This distribution is consistent with the normalized Exposure score exceeding the Pressure score across most of the mapped area. Because Exposure is derived from observed groundwater-level behaviour that may already contain anthropogenic effects, these proportions should not be interpreted as separating natural and human controls. The spatial coincidence between higher Pressure scores and mining-affected areas is consistent with a possible local influence of dewatering on groundwater conditions. Nevertheless, the present indicator-based analysis does not allow the climatic and anthropogenic contributions to observed SGI behaviour to be separated quantitatively.

6.5 Limitations and implications

Several limitations should be recognized. ~~Spatial~~ The monitoring network is relatively sparse, comprising 16 piezometers, including only two representing the deep confined aquifer. Consequently, group-level comparisons and spatial interpolation ~~adds~~ are subject to uncertainty ~~due to~~ , particularly in areas located far from observation wells and for the deep aquifer system. The resulting maps should therefore be interpreted as exploratory screening products rather than as spatially exhaustive or predictive representations.

SPI represents precipitation-deficit forcing but does not account explicitly for atmospheric evaporative demand, actual evapotranspiration, soil-moisture storage, snow processes, or effective recharge. Consequently, the SPI–SGI analysis does not provide a complete climatic water-balance attribution. Future work should incorporate SPEI, soil-moisture observations, and independently estimated recharge where sufficiently consistent data ~~density~~are available.

Monitoring periods and ~~method choice. The use~~the number of contributing wells varied through time. Group-level SGI series consequently represent dynamically supported aquifer-group means rather than strictly balanced-panel averages. This limitation is most relevant for the shallow group, which contains the largest number of wells and the greatest variation in record length. Differences among group-level SGI series may therefore partly reflect changes in temporal data support as well as hydrogeological contrasts.

The selected SGI aggregation ~~scales~~scale also affects the ~~depiction~~representation of drought duration, persistence, and ~~the pressure~~recovery. Longer aggregation windows smooth short-term variability and emphasize prolonged anomalies, whereas shorter windows identify more frequent and transient events. In addition, the lag associated with the maximum SPI–SGI correlation varied among subperiods and should not be interpreted as a fixed aquifer response time.

The Pressure component relies on simplified ~~indicators of~~ spatial proxies. Well density does not directly represent abstraction ~~and mining activity~~volumes, while the mining layer identifies potential influence zones without accounting for the temporal variability or intensity of dewatering. The component weights are expert-based and have not yet been externally calibrated. Although alternative weighting schemes provide a useful sensitivity check, they do not establish the robustness of individual mapped values or hotspot boundaries.

Because the groundwater-level records used to derive Exposure may already incorporate anthropogenic influences, Exposure and Pressure are neither statistically nor causally independent. The E−P contrast should therefore not be interpreted as separating intrinsic aquifer behaviour from human pressure, but only as a descriptive comparison of the relative mapped magnitudes of the two normalised components.

Leave-one-out cross-validation indicated substantial and spatially heterogeneous interpolation uncertainty. The highest errors occurred at isolated piezometers and where spatially adjacent wells represented different aquifer systems and strongly contrasting normalised drought metrics. Because the analysis uses a two-dimensional interpolation, it cannot explicitly account for vertical hydrogeological separation between overlapping shallow and deep aquifers. The uneven monitoring density, particularly the limited point support in the southern part of the study area, further reduces the reliability of local predictions. Accordingly, the mapped surfaces and area-based class summaries should be interpreted as exploratory screening outputs rather than precise regional estimates.

Despite these limitations, the ~~integrated~~ framework ~~offers a consistent foundation for connecting groundwater drought dynamics with spatial vulnerability patterns and~~ provides a ~~process-oriented approach for evaluating~~consistent and hydrogeologically informed basis for integrating observed groundwater drought ~~under combined climatic and human influences~~behaviour with spatial indicators of anthropogenic pressure and environmental sensitivity. Its main value lies in supporting comparative screening, identifying areas that may warrant closer investigation, and highlighting data and monitoring needs for future groundwater drought assessment.

7. Conclusions

This study ~~demonstrates that~~ identified contrasting groundwater drought ~~vulnerability in GWB 43 arises from the interactions~~behaviour among ~~climatic forcing,~~the three monitored aquifer ~~memory, anthropogenic pressure, and environmental sensitivity within a unified Drought Impact Potential Index (DIPI) framework. The results demonstrate that this objective has been successfully achieved.~~

~~The analysis reveals that~~systems in GWB 43. The shallow unconfined aquifer showed the strongest SPI–SGI association and generally shorter groundwater drought ~~behavior varies systematically across aquifer types. Shallow unconfined systems respond and recover quickly, while deeper~~episodes, whereas the deep confined ~~systems show~~aquifer exhibited delayed ~~effects, prolonged drought periods, and limited recovery. These variations are evident in drought metrics derived from SGI and suggest that aquifer storage and system memory are key factors influencing the persistence of groundwater droughts.~~

~~A key finding is the asymmetry between drought propagation and recovery. While spread is driven by the buildup of~~ meteorological association, prolonged SGI-12 deficits, ~~recovery needs ongoing recharge and is therefore significantly slower, particularly in deeper systems. This results in extended groundwater drought even after meteorological conditions improve, as shown in the analyzed time series and recovery metrics~~and no observed recovery within the available record. These contrasts are consistent with differences in storage, confinement, and hydraulic connectivity, but conclusions concerning the deep system remain exploratory because it is represented by only two piezometers and may also be influenced by sustained anthropogenic pressure.

The ~~spatial~~ analysis ~~indicates that the impact of~~ highlights an asymmetry between drought development and recovery. Groundwater deficits may persist after meteorological conditions improve because recovery depends on sustained recharge and groundwater ~~drought is mainly driven by inherent system properties.~~ storage restoration. Nevertheless, lagged SPI–SGI correlations describe empirical temporal associations and should not be interpreted as uniquely determined propagation times or causal process attribution.

The DIPI framework integrates piezometer-level groundwater drought characteristics with proxy indicators of anthropogenic Pressure and environmental Sensitivity. Weighted and equally weighted formulations produced broadly similar regional patterns, but leave-one-out cross-validation showed substantial interpolation uncertainty. The resulting maps are therefore suitable for comparative regional screening and identification of areas warranting further investigation, rather than for precise local prediction or delineation of robust hotspot boundaries.

The E−P contrast showed that mapped Exposure~~-dominated areas make up about 60~~ exceeded mapped Pressure across 65.5% of the study area, ~~while pressure-dominated zones (around 22%) are limited in size and mostly linked to mining-related~~values were near-balanced across 31.6%, and Pressure exceeded Exposure across 2.9%. These proportions represent descriptive mapped classes only. Because SGI-derived Exposure may already contain the effects of abstraction and mine dewatering~~. This indicates that human activities mainly serve as local boosters of drought, while~~, the ~~overall spatial pattern is controlled by aquifer-scale processes~~contrast does not separate climatic and anthropogenic controls.

The proposed ~~DIPI~~hydrogeologically informed statistical framework ~~proved robust to weighting assumptions and effectively captures the interaction among system response, anthropogenic pressure, and environmental sensitivity. By incorporating process-based drought metrics into the exposure component, the approach~~ provides a ~~physically grounded link between~~transparent basis for combining temporal groundwater drought ~~dynamics and~~ behaviour with spatial ~~vulnerability patterns, which is not explicitly represented in conventional static index-based approaches.~~

~~Although the pressure component relies on proxy~~screening indicators~~ rather than~~. Application in other groundwater systems would require local calibration, denser and more representative monitoring, direct ~~measurements of ~~abstraction ~~rates ~~and ~~mining ~~dewatering ~~volumes, the consistent spatial patterns suggest that the identified relationships accurately reflect strong system-scale controls. Overall, the results demonstrate that groundwater drought in GWB 43 cannot be explained solely by climatic forcing but must be understood as the outcome of interactions among meteorological conditions, aquifer properties, and human pressures. The proposed framework provides a transferable approach for assessing ~~data, and independent observations of groundwater drought ~~vulnerability in complex hydrogeological systems and offers a basis for improved groundwater management amid increasing climatic and human stresses~~impacts.

Appendix A

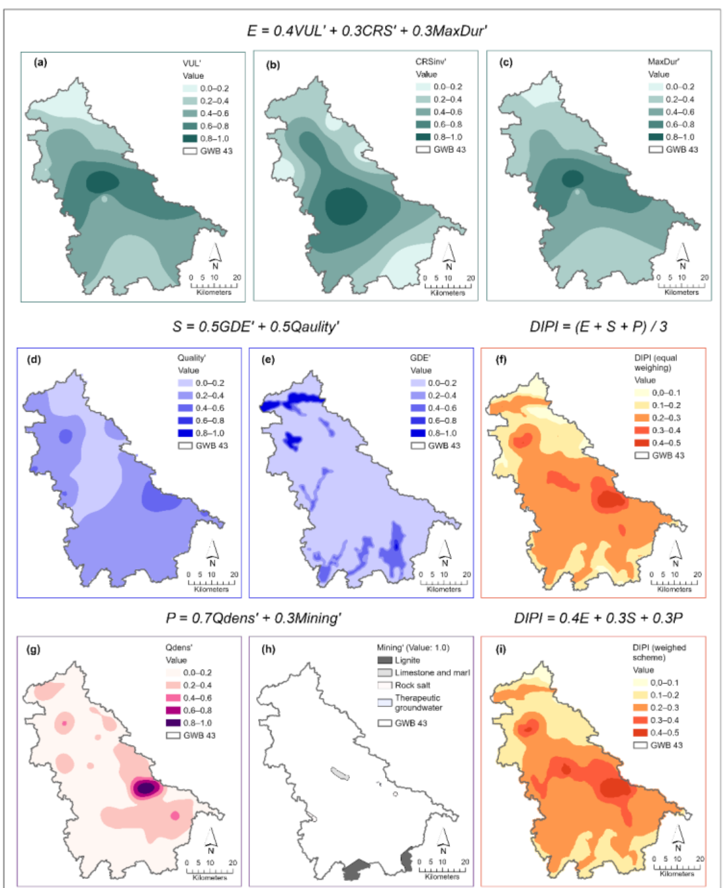

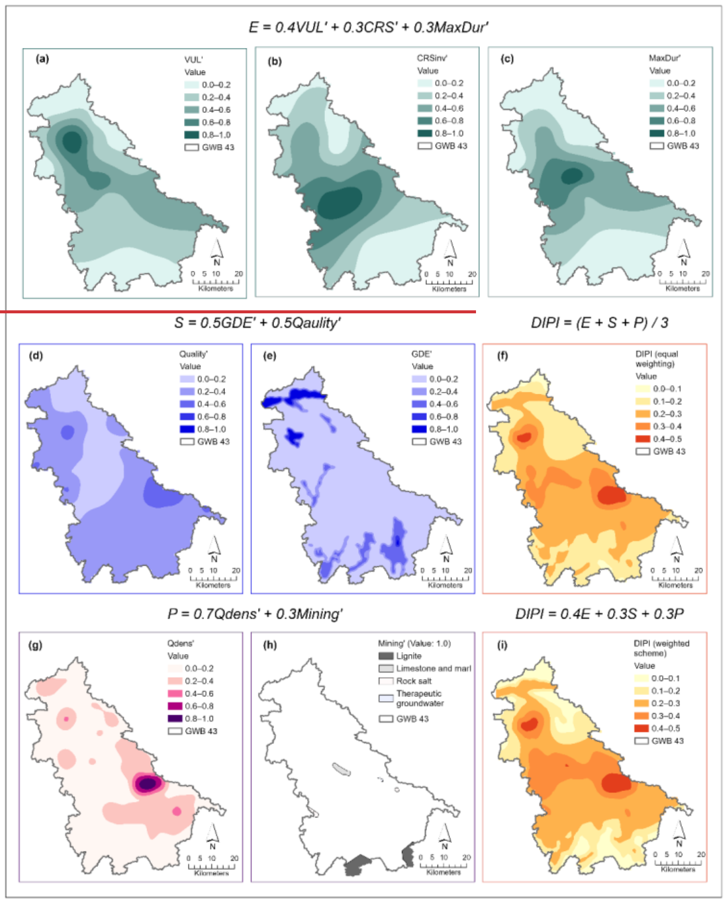

Figure A1: Spatial distribution of ~~normalized~~normalised DIPI sub-components and comparison of aggregation schemes. Panels (a–c) present the ~~normalized~~normalised exposure metrics (VUL′, CRSinv′, MaxDur′), panels (d–e) the sensitivity layers (Quality′, GDE′), and panels (g–h) the pressure layers (Qdens′, Mining′). Panels (f) and (i) compare the equally weighted and weighted DIPI variants, respectively, ~~highlighting the spatial robustness of hotspot patterns~~illustrating similarities and local differences between the two weighting schemes.

Appendix B

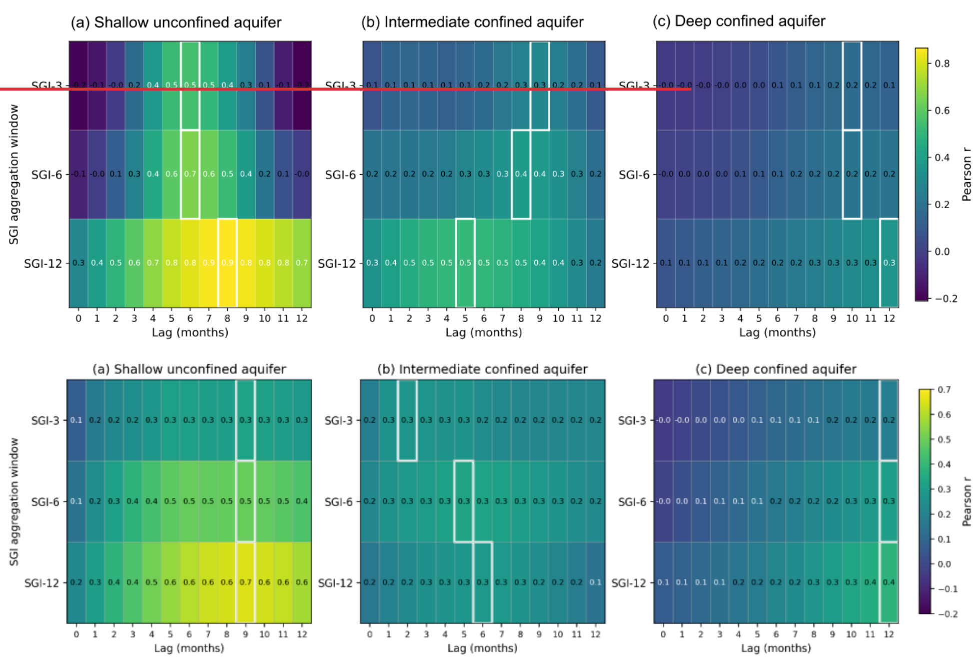

Figure B1~~: Lagged Pearson ~~. Full-period lagged SPI–SGI correlations for the three monitored aquifer systems in GWB 43. Panels show Pearson correlation coefficients between ~~SPI ~~aquifer-group mean SGI and ~~SGI for the three groundwater clusters:~~SPI from the meteorological station nearest to the corresponding aquifer-group centroid for (a) the shallow unconfined aquifer, (b) the intermediate confined aquifer, and (c) the deep confined aquifer. ~~Rows represent SGI~~ Correlations were calculated separately for the 3-, 6-, and 12-month aggregation ~~windows (3, 6, and 12~~scales over lags of 0–12 months~~), whereas columns represent SPI lags from 0 to ~~. White outlines mark the lag associated with the maximum correlation in each row. Positive lags indicate that SGI follows SPI. Maxima occurring at 12 months ~~based on the nearest precipitation station. The heatmaps reveal clear differences in drought propagation strength~~represent the upper boundary of the tested range and do not exclude longer response ~~timing among clusters, with the shallow unconfined aquifer showing the strongest and fastest~~delays.

Appendix C

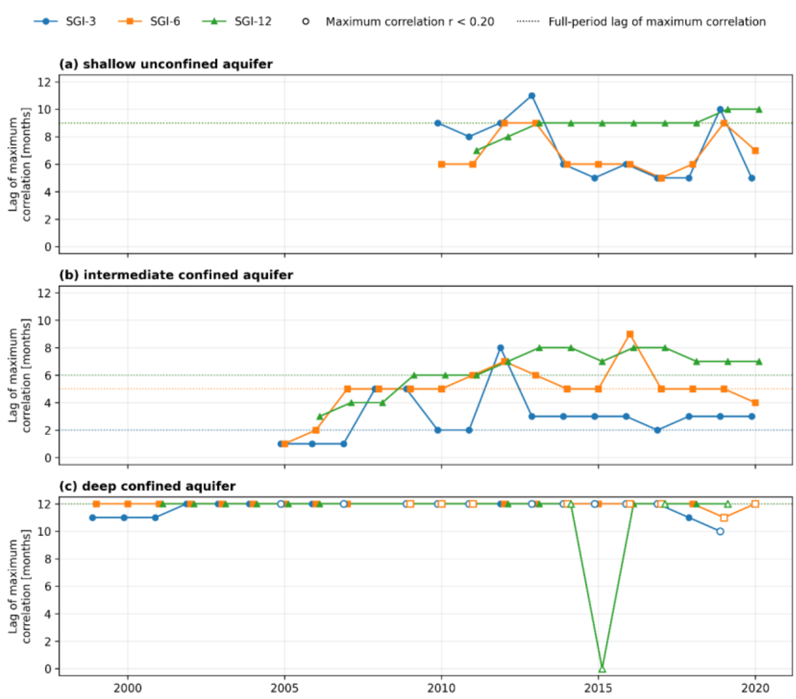

Figure C1. Temporal stability of the lag associated with the maximum SPI–SGI correlation in the three aquifer systems. The panels show results for (a) the shallow unconfined aquifer, (b) the intermediate confined aquifer, and (c) the deep confined aquifer, calculated using 10-year moving windows shifted forward by 1 year. Symbols indicate the lag of the maximum Pearson correlation for SGI-3, SGI-6, and SGI-12. Open symbols denote cases in which the maximum correlation was weak (r<0.20). Horizontal dotted lines are consistent with the full-period lag of maximum correlation for each SGI aggregation scale. Values reaching the upper tested limit of 12 months are consistent with the possibility that the actual response~~.~~ delay may exceed the analysed lag range.

Author contributions

KS designed the study concept and analytical framework, including the piezometer classification, drought-response metrics, and DIPI construction. KS performed the analyses, prepared all figures, interpreted the results, supervised the study, and wrote the manuscript. KJ compiled, curated, and quality-checked the original groundwater and meteorological datasets during the preceding MSc-level study and contributed to data validation in the present work. Both authors revised and approved the final manuscript.

Disclaimer

Copernicus Publications remains neutral with regard to jurisdictional claims made in the text, published maps, institutional affiliations, or any other geographical representation in this paper. While Copernicus Publications makes every effort to include appropriate place names, the final responsibility lies with the authors. Views expressed in the text are those of the authors and do not necessarily reflect the views of the publisher.

Acknowledgements

The authors acknowledge the Polish Geological Institute – National Research Institute (PIG-PIB) and the Polish Hydrogeological Survey for maintaining the national groundwater monitoring network and for providing access to the long-term piezometric records used in this study. Meteorological observations were provided by IMGW-PIB. Data processing and spatial analyses were supported by the GIS and computational facilities of the Faculty of Geology, University of Warsaw.

AI use statement

Generative AI tools (ChatGPT, Grammarly) were used exclusively for language refinement and stylistic editing of selected parts of the manuscript. All scientific interpretations, methodological decisions, calculations, and final text verification were performed by the authors.

Code and data availability

The ~~minimal~~ reproducible input datasets, processed analytical outputs, figure source data, ~~reproducible~~and Jupyter notebooks~~, and the master workflow description~~ used in this study are openly available ~~via~~in the GitHub repository (https://github.com/sawicka-byte/GWB43-groundwater-drought-DIPI) and archived as a versioned release on Zenodo (Sawicka and Jurzyk, 2026; https://doi.org/10.5281/zenodo.~~19371351).~~ 21471221).

The repository includes the monthly groundwater-level and precipitation inputs used in the analyses, revised SGI-3, SGI-6, and SGI-12 series, well- and aquifer-group drought events and metrics, propagation and recovery outputs, DIPI component tables, figure source data for the main text and Appendices A–C, and stepwise ~~preprocessing~~Jupyter notebooks reproducing the SGI, drought-metric, ~~DIPI construction, and figure-generation~~and DIPI workflows~~, along with a master reproducibility entry point that describes the full analytical chain.~~.

Raw institutional groundwater~~-~~-monitoring ~~data~~records from the Polish Hydrogeological Survey (PIG-PIB) are subject to access restrictions and cannot be redistributed. ~~To ensure full reproducibility, the~~The repository therefore provides the processed monthly monitoring series used as analytical inputs, together with all derived ~~standardized drought~~ indices, ~~drought~~ metrics, ~~DIPI components~~component tables, and figure source ~~tables~~data used directly in the ~~analyses~~study.

Competing interests

The authors declare that they have no conflict of interest.

Financial support

This research received no specific grant from any funding agency in the public, commercial, or not-for-profit sectors.

References

Barker, L. J., Hannaford, J., Chiverton, A., and Svensson, C.: From meteorological to hydrological drought using standardised indicators, Hydrol. Earth Syst. Sci., 20, 2483–2505, https://doi.org/10.5194/hess-20-2483-2016, 2016.

Berghuijs, W. R., Woods, R. A., and Hrachowitz, M.: Annual memory in the terrestrial water cycle, Hydrol. Earth Syst. Sci., 29, 1319–1335, https://doi.org/10.5194/hess-29-1319-2025, 2025.

Bloomfield, J. P., and Marchant, B. P.: Analysis of groundwater drought building on the standardised precipitation index approach, Hydrol. Earth Syst. Sci., 17, 4769–4787, https://doi.org/10.5194/hess-17-4769-2013, 2013.

Bloomfield, J. P., Marchant, B. P., McKenzie, A. A., and Lewis, M. A.: Regional analysis of groundwater droughts using hydrograph classification, Hydrol. Earth Syst. Sci., 23, 1397–1416, https://doi.org/10.5194/hess-23-1397-2019, 2019.

Chen, Y., Zhang, Y., Tian, J., Tang, Z., Wang, L., and Yang, X.: Understanding the propagation of meteorological drought to groundwater drought: a case study of the North China Plain, Water, 16, 501, https://doi.org/10.3390/w16030501, 2024.

Ebeling, P., Musolff, A., Kumar, R., Hartmann, A., and Fleckenstein, J. H.: Groundwater head responses to droughts across Germany, Hydrol. Earth Syst. Sci., 29, 2925–2950, https://doi.org/10.5194/hess-29-2925-2025, 2025.

Fiszer, J., and Derkowska-Sitarz, M.: Forecast of development of depression cone and water inflows to brown coal mine Konin, Hydrogeologia, 442, 5–24, 2010.

~~The Polish Geological Institute - National Research Institute (PGI-NRI): GWB 43 status card, https://www.pgi.gov.pl/dokumenty-pig-pib-all/psh/zadania-psh/jcwpd/jcwpd-40-59/4461-karta-informacyjna-jcwpd-nr-43/file.html, 2022.~~

Ghasempour, F., Yamaç, S. S., Sekertekin, A., Iban, M. C., and Kutoglu, S. H.: Spatiotemporal agricultural drought assessment and mapping its vulnerability in a semi-arid region exhibiting aridification trends, Agriculture, 15, 2060, https://doi.org/10.3390/agriculture15192060, 2025.

Gleeson, T., Wang-Erlandsson, L., Zipper, S. C., Porkka, M., Jaramillo, F., Gerten, D., and Famiglietti, J. S.: The water planetary boundary, Nature, 588, 257–261, https://doi.org/10.1038/s41586-020-2550-7, 2020.

Goovaerts, P.: Geostatistics for natural resources evaluation, Oxford University Press, Oxford, 1997.

Gorelick, S. M., and Zheng, C.: Global change and the groundwater management challenge, Water Resour. Res., 51, 4409–4438, https://doi.org/10.1002/2015WR017466, 2015.

Guttman, N. B.: Accepting the standardized precipitation index: a calculation algorithm, J. Am. Water Resour. Assoc., 35, 311–322, https://doi.org/10.1111/j.1752-1688.1999.tb03592.x, 1999.

Hengl, T.: A practical guide to geostatistical mapping, European Commission, Luxembourg, 2009.

Hisdal, H., Tallaksen, L. M., and Clausen, B.: Hydrological drought characteristics, in: Drought: a global assessment, edited by: Wilhite, D. A., Routledge, London, 2001.

Hutchinson, M. F.: A new procedure for gridding elevation and stream line data with automatic removal of spurious pits, *Journal of Hydrology*, 106, 211–232, https://doi.org/10.1016/0022-1694(89)90073-5, 1989.

Jasechko, S.: Global cases of groundwater recovery after interventions, Science, 391, 1218–1228, https://doi.org/10.1126/science.adu1370, 2026.

Jiao, D., Wang, D., and Lv, H.: Effects of human activities on hydrological drought patterns in the Yangtze River, China, Nat. Hazards, 104, 1111–1124, https://doi.org/10.1007/s11069-020-04206-2, 2020.

Jurzyk, K.: Zagrożenie suszą hydrogeologiczną w rejonie JCWPd 43 przy słabym stanie ilościowym wód podziemnych, MSc thesis, University of Warsaw, Warsaw, Poland, 74 pp., 2025.

Kartal, V., and Nones, M.: Assessment of meteorological, hydrological and groundwater drought in the Konya closed basin, Türkiye, Environ. Earth Sci., 83, 285, https://doi.org/10.1007/s12665-024-11587-1, 2024.

Kumar, R., Musuuza, J. L., Van Loon, A. F., Teuling, A. J., Barthel, R., and Broek, J. T.: Multiscale evaluation of the standardized precipitation index, Hydrol. Earth Syst. Sci., 20, 1117–1131, https://doi.org/10.5194/hess-20-1117-2016, 2016.

Ling, Z., Shu, L., Wang, D., Lu, C., and Liu, B.: Assessment and projection of groundwater drought vulnerability under different climate scenarios and land use changes in the Sanjiang Plain, China, J. Hydrol. Reg. Stud., 49, 101498, https://doi.org/10.1016/j.ejrh.2023.101498, 2023.

McKee, T. B., Doesken, N. J., and Kleist, J.: The relationship of drought frequency and duration to time scales, in: Proc. 8th Conf. Applied Climatology, American Meteorological Society, Boston, 179–184, 1993.

Li, J. and Heap, A.D.: A Review of Spatial Interpolation Methods for Environmental Scientists. Geoscience Australia, Record 2008/23, 137, 2008.

Nowak, B., Szadek, P., Szymański, K., and Lawniczak-Malińska, A.: Concept and implementation of solutions improving water relations in the area of the flooded opencast lignite mine Kazimierz Północ (Central-West Poland), Water, 15, 706, https://doi.org/10.3390/w15040706, 2023.

Peters, E., Torfs, P. J. J. F., Van Lanen, H. A. J., and Bier, G.: Propagation of drought through groundwater – a new approach using linear reservoir theory, Hydrol. Earth Syst. Sci., 7, 112–123, https://doi.org/10.5194/hess-7-112-2003, 2003.

Polish Geological Institute - National Research Institute (PGI-NRI): GWB 43 status card, https://www.pgi.gov.pl/dokumenty-pig-pib-all/psh/zadania-psh/jcwpd/jcwpd-40-59/4461-karta-informacyjna-jcwpd-nr-43/file.html, 2022.

Porter, J. R., Xie, L., Challinor, A. J., Cochrane, K., Howden, S. M., Iqbal, M. M., Lobell, D. B., and Travasso, M. I.: Food security and food production systems, in: Climate Change 2014: Impacts, Adaptation, and Vulnerability. Part A: Global and Sectoral Aspects, Cambridge University Press, Cambridge, 485–533, 2014.

Przybyłek, J.: Dewatering problems in lignite mines, Górnictwo Odkrywkowe, 59, 5–14, 2018.

Risk, C., James, P. M. A., and Metsaranta, J. M.: Optimal cross-validation strategies for selection of spatial interpolation models for the Canadian Forest Fire Weather Index System, *Earth and Space Science*, 9, e2021EA002019, https://doi.org/10.1029/2021EA002019, 2022.

Saha, S., Gogoi, P., Gayen, A., and Chandra, G. P.: Constructing a machine-learning-based spatial drought vulnerability index in Karnataka state of India, J. Clean. Prod., 314, 128073, https://doi.org/10.1016/j.jclepro.2021.128073, 2021.

Sawicka, K., and Jurzyk, K.: ~~Reproducible workflows and processed datasets for~~ GWB43-groundwater~~-~~-drought ~~vulnerability assessment in GWB 43 (Version~~ DIPI: Add Exposure interpolation and cross-validation outputs, version 1.~~0),~~3, Zenodo, https://doi.org/10.5281/zenodo.21471221, 2026.

Shukla, S., and Wood, A. W.: Use of a standardized runoff index for characterizing hydrologic drought, Geophys. Res. Lett., 35, L02405, https://doi.org/10.1029/2007GL032487, 2008.

Tallaksen, L. M., and Van Lanen, H. A. J.: Hydrological drought: processes and estimation methods for streamflow and groundwater, Elsevier, Amsterdam, 2004.

Teutschbein, C., Grabs, T., Giese, M., Todorović, A., and Barthel, R.: Drought propagation in high-latitude catchments: insights from a 60-year analysis using standardized indices, Nat. Hazards Earth Syst. Sci., 25, 2541–2564, https://doi.org/10.5194/nhess-25-2541-2025, 2025.

Thomas, B. F., and Famiglietti, J. S.: Groundwater depletion, Geophys. Res. Lett., 44, 11445–11455, https://doi.org/10.1002/2017GL075965, 2017.

Van Loon, A. F.: Hydrological drought explained, WIREs Water, 2, 359–392, https://doi.org/10.1002/wat2.1085, 2015.

Van Loon, A. F., Stahl, K., Di Baldassarre, G., Clark, J., Rangecroft, S., Wanders, N., Gleeson, T., Van Dijk, A. I. J. M., Tallaksen, L. M., Hannaford, J., Uijlenhoet, R., Teuling, A. J., Hannah, D. M., Sheffield, J., Svoboda, M., Verbeiren, B., Wagener, T., and Van Lanen, H. A. J.: Drought in a human-modified world: reframing drought definitions, understanding, and analysis approaches, Hydrol. Earth Syst. Sci., 20, 3631–3650, https://doi.org/10.5194/hess-20-3631-2016, 2016.

Willmott, C. J. and Matsuura, K.: On the use of dimensioned measures of error to evaluate the performance of spatial interpolators, International Journal of Geographical Information Science, 20, 89–102, 2006.

Vega Briones, J., Sutanudjaja, E. H., de Jong, S., and Wanders, N.: Modelling groundwater hydrological drought and its recovery given natural and anthropogenic scenarios in South America, Hydrol. Process., 38, e15340, https://doi.org/10.1002/hyp.15340, 2024.

Vicente-Serrano, S. M., Beguería, S., and López-Moreno, J. I.: A multiscalar drought index sensitive to global warming: the standardized precipitation evapotranspiration index, J. Climate, 23, 1696–1718, https://doi.org/10.1175/2009JCLI2909.1, 2010.

Wheater, H. S., and Evans, E. J.: Land use and flood risk, Land Use Policy, 26, S251–S264, https://doi.org/10.1016/j.landusepol.2009.08.007, 2009.

World Meteorological Organization: Standardized precipitation index user guide (WMO-No. 1090), WMO, Geneva, 2012.

Zhu, R., Zheng, H., and Jakeman, A. J.: Groundwater drought variability and its propagation, Water Resour. Res., 58, e2021WR030841, https://doi.org/10.1029/2021WR030841, 2022.